공학석사 학위논문

Ferrohydrodynamic System for Energy Harvesting

에너지 하비스팅을 위한

페로다이나믹 시스템

2013년 8월

서울대학교 대학원

재료공학부

윤 혜 림

Ferrohydrodynamic System for Energy Harvesting

에너지 하비스팅을 위한 페로다이나믹 시스템

지도 교수 윤 재 륜

이 논문을 공학석사 학위논문으로 제출함
2013 년 8월

서울대학교 대학원
재료공학부
윤 혜 림

윤혜림의 석사 학위논문을 인준함
2013년 8월

위 원 장 강 태 진 (인)

부위원장 윤 재 륜 (인)

위 원 유 웅 렬 (인)

Ferrohydrodynamic System for Energy Harvesting

Advisor: Jae Ryoun youn

by
Hye Lim Yun

2013

Department of Materials Science and Engineering

Graduate School

Seoul National University

ABSTRACT

Energy harvesting has been of keen interest to researchers and many energy harvesting methods were reported recently. In particular, there has been growing interest in an energy harvesting method which is based on electromagnetic energy. Most of the energy harvesters have been developed in the laboratory without practical applications. A ferrohydrodynamic system which utilizes movement of air droplets in a ferrofluid is proposed as an energy harvesting platform in this study. According to Faraday's law, relative motion under a magnetic field can cause a change of magnetic flux, which induces electromotive force in the surrounding coils. A ferrohydrodynamic system was prepared to investigate possibility of energy harvesting through Faraday's law.

Ferrohydrodynamically induced voltage and current were measured as a function of the flow rate of air, the magnetic field(H), and the magnetization(M). First, it was observed that the measured output current and voltage were in the same range regardless of the flow rate of air. Second, it was observed that as the magnetic field was increased by changing the number of magnets, output voltage and current increased. Finally, output voltage and current were measured by using two types of ferrofluid which consist of different saturation magnetization. It was observed that as saturation magnetization of a ferrofluid increased, output current and voltage

were increased. Numerical simulation with the commercial code, COMSOL, demonstrated that the ferryhydrodynamic system generates output voltage and current as expected. Magnetorheological and magnetodynamic effects of the ferrofluid on energy harvesting were characterized in this study. It was found that the ferrofluid showed shear thinning behavior and magnetoviscous effect under magnetic field.

Keywords: ferrohydrodynamic, magnetorheological fluid, ferrofluid, energy harvesting, electromagnetism

Student number: 2011-23319

CONTENTS

ABSTRACT

LIST OF FIGURES AND TABLES

I. INTRODUCTION

1.1. Magnetic materials

1.1.1. Classification of Magnetic Materials

1.1.2. Ferrofluid

1.2. Magnetic theory

1.3. Electromagnetism

1.3.1. Faraday’s law of induction

1.3.2. Electromagnetic-based energy harvesting application

1.4. Objective of this study

II. EXPERIMENTS

2.1. Materials

2.2. Experimental Setup

2.3. Characterization of ferrofluid

2.3.1. Rheological measurement

2.3.2. Thermogravimetric analysis

2.3.3. High Resolution Transmission Electron Microscope

2.4. Magnetic field measurement

2.5. Voltage and current measurement

2.6. High speed camera observation

Ⅲ. RESULTS AND DISCUSSION

3.1. Characterization

3.1.1. Morphology of ferrofluid

3.1.2. Thermogravimetric analysis

3.1.3. Magnetic field measurement

3.2. Rheological properties of ferrofluid

3.2.1. Shear thinning behavior

3.2.2. Magnetoviscous effect

3.2.3. Theoretical model of yield stress

3.3. Output voltage and current

3.3.1. Effect of the flow rate of the air

3.3.2. Effect of the magnetic field (H)

3.3.3. Effect of the magnetization (M)

3.4. Visualization of an air-droplet movement

3.5. Numerical simulation

3.5.1. Governing equations

3.5.2. Homogenization of the calculation domain

3.5.3. Numerical solutions

Ⅴ. CONCLUSION

REFERENCES

KOREAN ABSTRACT

LIST OF FIGURES AND TABLES

Figure 1.1. The direction of electron spins

Figure 1.2. Direction of the magnetic moment

Figure 1.3. Schematic of components of a ferrofluid

Figure 1.4. Domain of ferromagnetic and superparamagnetic particles

Figure 1.5. Dynamic a ferrofluid sculpture under magnetic field

Figure 1.6. Illustration of the effect of introducing a conductor as a core into a solenoid

Figure 2.1. Experimental setup

Figure 2.2. A setup for measuring magnetic flux density

Figure3.1. High Resolution-TEM image of ferrofluids

Figure 3.2. TGA curves of investigated ferrofluids

Figure 3.3. Variation in viscosity with shear rate at various magnetic fields for EFH-1

Figure 3.4. Variation in viscosity with shear rate at various magnetic fields for EFH-3

Figure 3.5. Shear rate VS viscosity for different magnetic fields with increasing magnetic field

Figure 3.6. The origin of a field dependent increase of viscosity in a ferrofluid

Figure 3.7. Magnetoviscous effect with various magnetic field

Figure 3.8. Shear stress versus shear rate in the absence of the magnetic field

Figure 3.9. Viscosity versus shear rate under different magnetic fields

Figure 3.10. Shear stress of EFH-1 for different magnetic fields by using Bingham model

Figure 3.11. Shear stress of EFH-3 for different magnetic fields by using Bingham model

Figure 3.12. Shear stress of EFH-1 for different magnetic fields by using the Casson model

Figure 3.13. Shear stress of EFH-3 for different magnetic fields by using the Casson model

Figure 3.14. Shear stress of EFH-1 for different magnetic fields by using the Herschel–Bulkley model

Figure 3.15. Shear stress of EFH-3 for different magnetic fields by using the Herschel–Bulkley model

Figure 3.16. A schematic showing the distribution of the magnetic dipoles in the ferrofluid for different flow rate of air

Figure 3.17. Effect of the flow rate of air on output current

Figure 3.18. Effect of the flow rate of air on output voltage

Figure 3.19. A schematic showing the distribution of the magnetic dipoles in a ferrofluid for different magnetic field

Figure 3.20. Effect of the the magnetic field on output current

Figure 3.21. Effect of the magnetic field on output voltage

Figure 3.22. Effect of the magnetization on output current

Figure 3.23. A comparison between viscosity of PEO and the ferrofluid

Figure 3.24. Illustration of formation of an air-droplet in aqueous solution of PEO

Figure 3.25. Illustration of simulation domain: The colored region represented

Figure 3.26. Illustration of a homogenization process

Figure 3.27. Magnetic flux density and magnetic flux field over time

Figure 3.28. (a) Experimental and (b) simulation results of induced voltage over time.

Table 3.1. Bingham fit parameters for EFH-1

Table 3.2. Bingham fit parameters for EFH-3

Table 3.3. Casson fit parameters for EFH-1

Table 3.4. Casson fit parameters for EFH-3

Table 3.5. Herschel-Bulkley fit parameters for EFH-1

Table 3.6. Herschel-Bulkley fit parameters for EFH-3

Ⅰ. INTRODUCTION

1.1. Magnetic material

1.1.1. Classification of Magnetic Materials

The magnetic behavior of materials is generally classified into five types: diamagnetic, paramagnetic, ferromagnetic, ferromagnetic, and anti-ferromagnetic behaviors depending on their magnetic susceptibilities. The two most common types of the magnetic materials are diamagnetic and paramagnetic materials. As seen in Fig.1.1-(a), diamagnetic materials consist of the full shell of electrons; that is, there are many upward spins and downward spins and the orbit and spin magnetic moments cancel out. Therefore, net magnetic moment will be zero in the absence of an external magnetic field. However, an applied field causes the spin moment to slightly exceed the orbital moment, resulting in a small net magnetic moment which opposes the applied field.

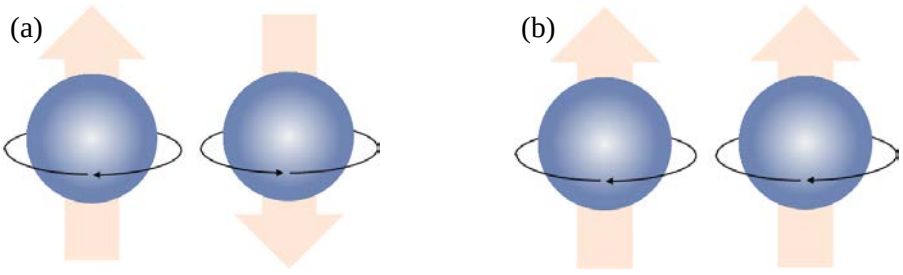

Figure 1.1. The direction of electron spins (a) Diamagnetic particles (b) Paramagnetic particles

Thus, if a diamagnetic material is brought near either pole of a strong magnet, it will be repelled as shown in Fig.1.2. A diamagnetic material has a relative magnetic permeability that is less than or equal to unity, resulting in a magnetic susceptibility becomes less than 0 since the susceptibility is defined as $\chi_m = \mu_r - 1$. This means that a diamagnetic materials is repelled by magnetic fields.

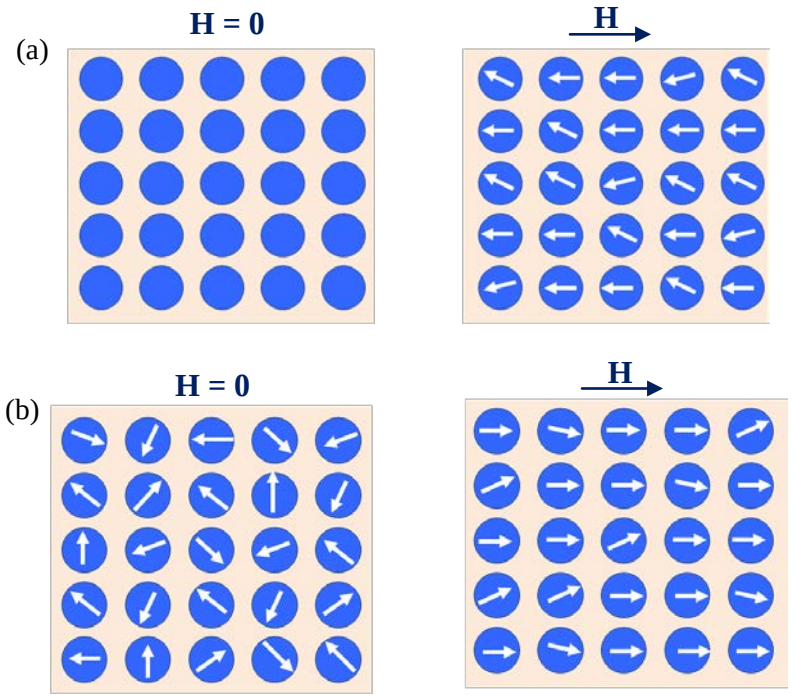

Figure 1.2. Direction of the magnetic moment (a) Diamagnetic material (b) Paramagnetic material.

Unlike diamagnetic materials, paramagnetic materials consist of unfilled electron shell. Because of the Pauli Exclusion Principle that no two electrons can have the same quantum number, there should be unpaired

electrons for unfilled shells of atoms. Thus, the electron spin and orbital motion do not quite cancel out. The atom as a whole has a small magnetic moment, but the random orientation of the atoms in material produces an average zero magnetic moment. Therefore, the paramagnetic materials show no magnetic effect in the absence of an external magnetic field. Under the external magnetic field, however, there is a small torque on each atomic moment and these moments tend to become aligned along an external field. This alignment acts to increase the value of magnetic field within the material. A paramagnetic materials has a relative magnetic permeability greater or equal to unity and magnetic susceptibility becomes greater than 0, which produces a paramagnetic material is attracted to the applied magnetic fields.

1.1.2. Ferrofluid

A ferrofluid is a kind of colloidal suspensions which is basically composed of magnetic particles, surfactant and carrier fluid as shown in Fig.1.3. The magnetic particles are typically magnetite or hematite on the order of tens of nanometers in diameter. The particles are coated with surfactant to prevent particle agglomeration with or without magnetic field to the ferrofluid. The surfactant is selected according to the type of carrier fluid to overcome the Van der Waals force and magnetic force between the particles. The carrier liquid is typically an oil- or water-based medium. [1]

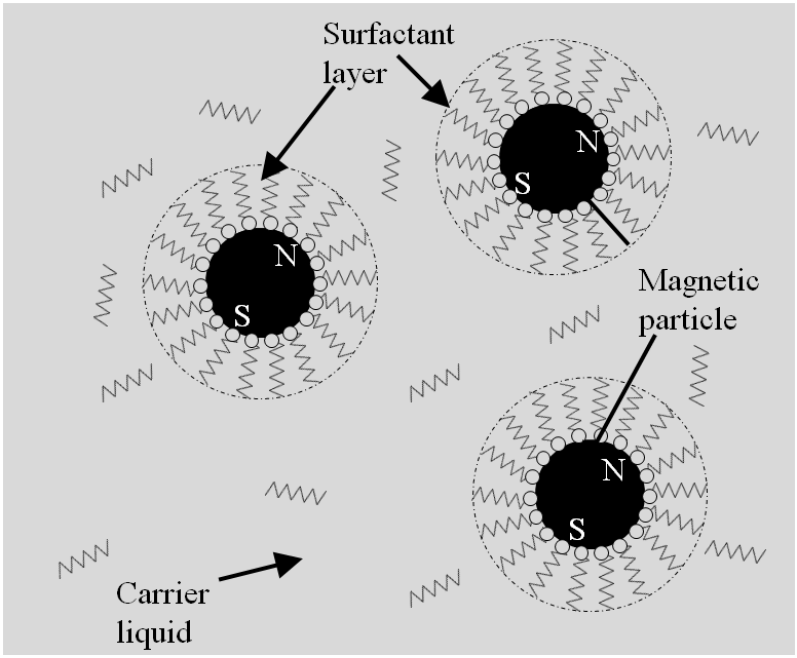

Figure 1.3. Schematic of components of a ferrofluid

A ferrofluid consists of ferromagnetic materials. The Ferromagnetic materials have unpaired electrons like paramagnetic materials. However, in ferromagnetic materials, electrons of atoms are grouped into domains where each domain has the same charge. In the absence of an external magnetic field, the electrons of atoms are organized into domains but, in the presence of a magnetic field these domains are aligned along the direction of the applied magnetic field so that charges are parallel throughout the entire compound as shown in Fig1.4.

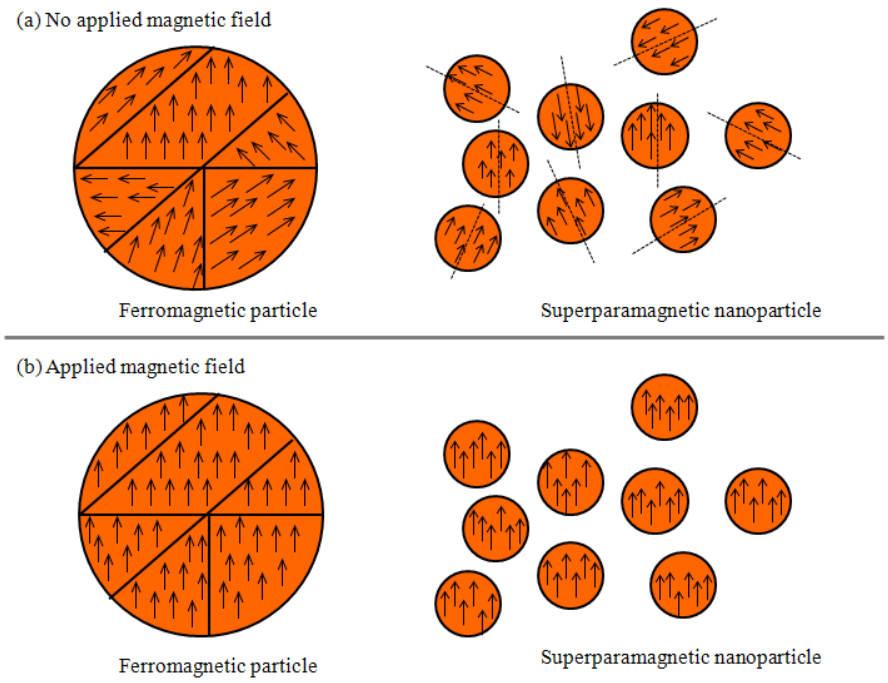

Figure 1.4. Domain of ferromagnetic and superparamagnetic particles

Although a ferrofluid consists of ferrimagnetic materials, it belongs to the class of materials defined as superparamagnetic. Since ferromagnetic materials are downsized to the nano-scale, these effectively act as single domain particles. These particles become magnetically unstable due to the thermal fluctuations and magnetization, and so can randomly flip their direction under the influence of temperature due to the thermomagnetic convection [2]. The response time between two flips is called the Néel relaxation time. Since the Néel relaxation time is an exponential function of the grain volume, it becomes obvious that flipping probability should be non-negligible for single domain particles.

In the absence of an external magnetic field, as measurement time for the magnetization of the nanoparticles is much longer than the Néel relaxation time, the magnetization appears to be zero. In this view, an external magnetic field is able to magnetize the nanoparticles similarly to paramagnetic materials. However, their magnetic susceptibility is much larger than the value of paramagnetic materials. [3]

Generally, a ferrofluid has been used in many applications ranging from sealing, damping, sensing, and drug-delivery agents.[4]

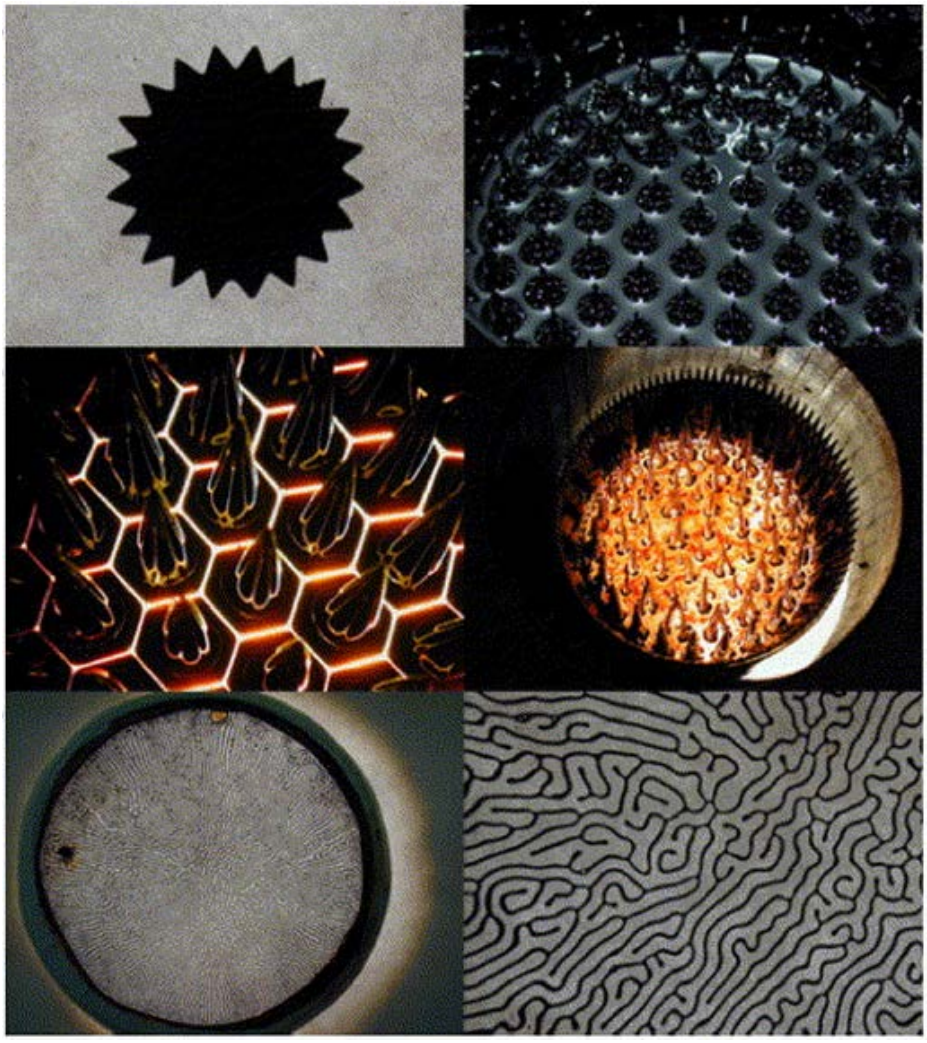

Figure 1.5. Dynamic a ferrofluid sculpture under magnetic field [5]

1.2. Magnetic theory

A magnetic field is produced by electrical charges in motion. Suppose that a magnetic field is generated by the solenoid without core flux through cylindrical conductors as shown in Fig.1.6-(a). In that case, it can be defined by the relationship $B=\mu_0 H$, where μ_0 is the magnetic permeability of the air ($\mu_0= 4\pi \times 10^{-7}$ Tm/A), B is the magnetic flux density, and H is the magnetic field.

As seen in Fig.1.6-(b), if the magnetic conductors like cylindrical metal iron are placed inside the core of solenoid, the magnetic flux density (B) will be increased due to that fact that the magnetic material themselves contributes internal magnetic field. Therefore, the magnetization (M) is contributed to the magnetic field (H), resulting in the final expression of the total magnetic field becomes $B=\mu_0(H+M)$. It means that ambiguities can arise about what part of the magnetic field comes from the external currents and the material itself. [6]

The relationship between the magnetization (M) and magnetic field (H) is given by $M= \chi_m H$ (χ_m is called the magnetic susceptibility). The magnetic susceptibility describes the degree of magnetization of a material in response to an applied magnetic field. A large value of χ_m corresponds to the strong magnetic material, while a small value of χ_m corresponds to the weak magnetic material.

Thus we have $B=\mu_0(H+\chi_m H)=\mu_0\mu_r H$ where $\mu_r=1+\chi_m$ is defined as the relative permeability. $\mu=\mu_0\mu_r$ is usually called an absolute permeability or often just a permeability. And this enables us to write the simple relationship between B and H.

$$\mathbf{B}=\mu\mathbf{H}$$

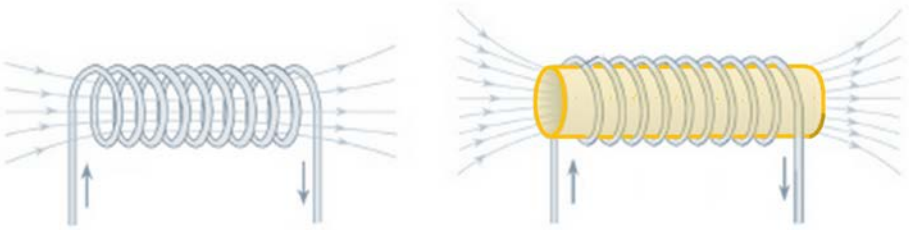

Figure 1.6. Illustration of the effect of introducing a conductor as a core into a solenoid (a) without a conductor and (b) with a conductor.

1.3. Electromagnetism

1.3.1. Faraday's law of induction

Faraday discovered an electromagnetic induction known as Fararaday's law of induction in which an electric field would be generated as a magnetic field changes with respect to time. It was also discovered that an electric current is generated significantly in a closed wire-loop as a magnetic material is moved through the closed wire-loop [7]. The equation of faraday's law of induction is as follows. This is a basic law of electromagnetism that predicts how a magnetic field interacts with an electric circuit.

$$\varepsilon = \oint \vec{E} \cdot d\vec{\ell} = -\frac{d}{dt}\Phi_B = -\frac{d}{dt}\int B \cdot d\vec{A}$$

where ε is the induced electromotive force (Φ_B) with regard to the time rate of change of the magnetic flux. The induced electromotive force is defined as $\Phi_B = \int BdA = BA\cos\theta$, where B is the magnetic flux density, A is the area of the surface and θ denotes the angle between B and normal to the plane. The negative sign in the equation is the direction of induced current. This law elucidates that the induced electromotive force in a closed loop equals to the magnetic flux with the time rate through the loop. In other words, relative motions under a magnetic field cause a change of magnetic flux, which induces the electromotive force in the coils.

1.3.2. Electromagnetic-based energy harvesting application

Electromagnetic generators are based on harvesting energy from motion and vibration sources of the system. By changing a magnetic field, electromagnetic generators induce an AC voltage across the coil [8]. One of the most effective methods for electromagnetic energy harvesting is to produce magnetic induction by means of permanent magnets, a coil, and a resonating cantilever beam. Rotating electromagnetic generators are in common use for generating power of a few watts to several hundred megawatts. It is possible to implement a damper of a micro-generator according to the faraday's law.

Typically, a mass-spring damper system is used to simulate the output power of electromagnetic generators. Actually, electromagnetic generators are used as a commercial device which has been developed by Kinetron, a Dutch manufacturer of precision electromechanical products. They have developed an electromagnetic rotational generator which can be used in applications such as self-powered pedal lights for bicycles. [9~10]

1.4. Objective of this study

In this paper, we reported a technique that utilizes movement of air-droplets in the ferrofluid under a magnetic field to convert energy to electric current and voltage via ferrohydrodynamics. The ferrohydrodynamic system is based on a liquid material known as a ferrofluid, which can easily be manipulated with external forces such as hydrodynamic and magnetic forces. In addition, this system gives an output voltage and current in response to very small changes in motion. The output voltage is induced within the coil according to the Faraday's law of induction. For comprehensive understanding in regard to physical parameters for the energy harvesting, we take account of a few experimental factors such as the flow rate of air-droplet, the magnetic field(H) and the magnetization(M) of the ferrofluid..

The ferrofluids were characterized by TGA, TEM, and rheometer to compare the material properties between EFH-1 and EFH-3 ferrofluid. Particularly, we focused on the magnetorheological and magnetodynamic effects on both of them because they have magnetic nanoparticles forming nanoclustering and chain-like structure under a magnetic field.

Ⅱ. EXPERIMENTAL

2.1. Materials

Commercially available ferrofluids purchased from Ferrotec, USA were used for the experiment. Two kinds of ferrofluids (EFH-1 and EFH-3) with different contents of magnetite particles were used. One type of ferrofluids was EFH-1 with the corresponding properties: the fluid mass density ρ = 1210 kg/m^3, the dynamic viscosity η = 6 cP, the size of suspension d = 5-10 mm, and the saturation magnetization M_s = 440 Gauss. Second is hydrocarbon-based EFH-3 with the corresponding properties: the fluid mass density ρ = 1420 kg/m^3, the dynamic viscosity η = 12 cP, the size of suspension d = 5-10 mm, and the saturation magnetization M_s = 650 Gauss.

To visualize formation and movement of air-droplets, PEO with molecular weight 1,000,000 was used to represent the behavior of air-droplets in the ferrofluids because the formation and movement of air-droplets are invisible due to non-transparency of the ferrofluids. PEO was mixed with distilled water in specific concentration (70 ppm) by using sonication for a few minutes at 80℃ to make viscous materials similar to those of the ferrofluids.

2.2. Experimental Setup

A cylindrical syringe with a diameter of 20 mm and a height of 90 mm was used as a container of ferrofluids. The mass of ferrofluids inside of the syringe was kept 2 ml. A copper coil with a diameter of 0.3 mm was wrapped hundreds of times around the container so as to be used as a solenoid. Finally, the cross section of the multi-turn coil was about $0.785 cm^2$.

To generate external magnetic field, NdFeB magnets with a dimension of 400 mm × 250 mm × 100 mm were used. In order to prevent the strong attraction between the magnets, An acrylic jig with 6.5 cm × 8 cm × 11.5 cm was designed as shown in Fig.2.1. A pair of permanent magnets was placed onto the side of the solenoid. A syringe pump was used to inject air into the ferrofluids and to make an air-droplet. The flow rate of air was controlled by the syringe pump.

Figure 2.1. Experimental setup

2.3. Characterization of ferrofluid

2.3.1. Rheological measurement

A measurement of rheological properties of ferrofluids is important to understand fundamental insights for magnetoviscous effects. Rheological properties were measured using rheometer (Anton Paar MCR 301, Ostfildern, Germany) with a parallel plate. The magnetic field and shear rate are controlled by the rheometer. Apparent viscosity of the ferrofluids was measured as a function of shear rate over the range of 0–500 s^{-1} at electric field range from 0 A to 5 A. The relationship between current (I) applied to the samples and magnetic flux density (B) is known to be $B \fallingdotseq 220 \times I$. In this experiment, the applied current varies from 0 A to 5 A, for which the intensity of magnetic field is 0 mT to 1100 mT.

Prior to the measurements, the ferrofluids were sonicated for approximately 10 min to disperse ferromagnetic particles.

2.3.2. Thermogravimetric analysis

Thermogravimetric analysis (TGA, Model 2950 TGA V5.4A) was used to measure the amount of magnetic particles in ferrofluid. A measurement was performed under a nitrogen atmosphere from room temperature to 800 ℃ with increasing the temperature by 10 °C/min.

2.3.3. High Resolution Transmission Electron Microscope

To obtain morphological information of ferrofluids and the size of nanoparticles, high-resolution transmission electron microscopy (JEM-3000F) with an accelerating voltage of 30kV was used. The samples were prepared by placing a drop of very dilute ferrofluid onto a copper grid and dried.

2.4. Magnetic field measurement

A gauss meter (LakeShore® 455 DSP) with axial probe from the same manufacture was used to measure the magnetic flux density. And the calibration had been realized with the Zero Gauss Chamber (model 4060). The gaussmeter probe was placed between the NdFeB magnets with the probe tip located at the center to ensure the symmetry of the magnetic field from the NdFeB magnets as shown in Fig.2.2.

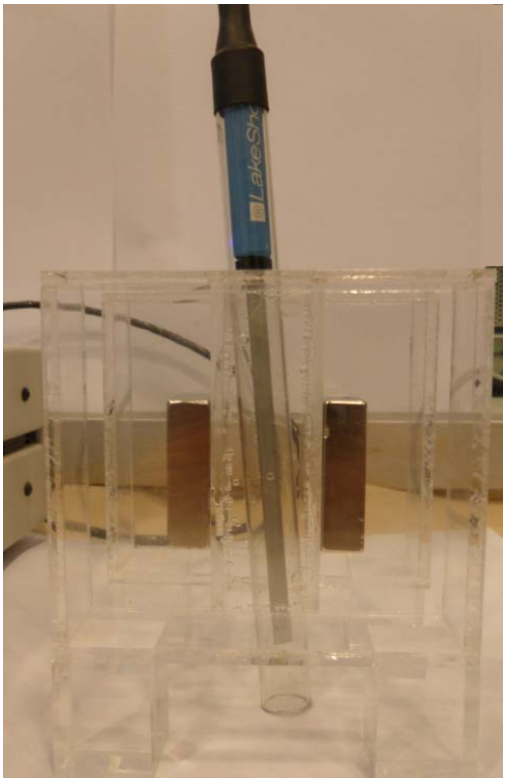

Figure 2.2. A setup for measuring magnetic flux density.

2.5. Voltage and current measurement

Induced voltage was measured with a nanovoltmeter (Keithley 2182A) and current was measured with a potentiostat (VersaSTAT^3). The nanovoltmeter and potentiostat were connected to a personal computer for sampling and storing the data automatically. The experimental setup was enclosed in a faraday cage to confirm the barrier from any external sources affecting the external electric field.

One side of the winding coil acts as a positive terminal and the other side acts as a negative terminal and both were connected by the crocodile clips.

2.6. High speed camera observation

The shape, size, and generating frequency of an air-droplet were visualized and recorded by a high speed camera (X-Stream ^{TM} Vision, XS-4). This equipment supports a maximum resolution of 512×512 pixels with 5,100 frames per second. For this study, recording rate of 100 frames per second was used during the visualization for observing the dynamic droplet behavior.

Ⅲ. RESULTS AND DISCUSSION

3.1. Characterization

3.1.1. Morphology of ferrofluid

Fig.3.1 shows spherical magnetite colloidal aggregates covered with surfactant. From the obtained HR-TEM image, it is shown that the sizes of the both EFH-1 and EFH-3 were in the range 5 nm to 10 nm.

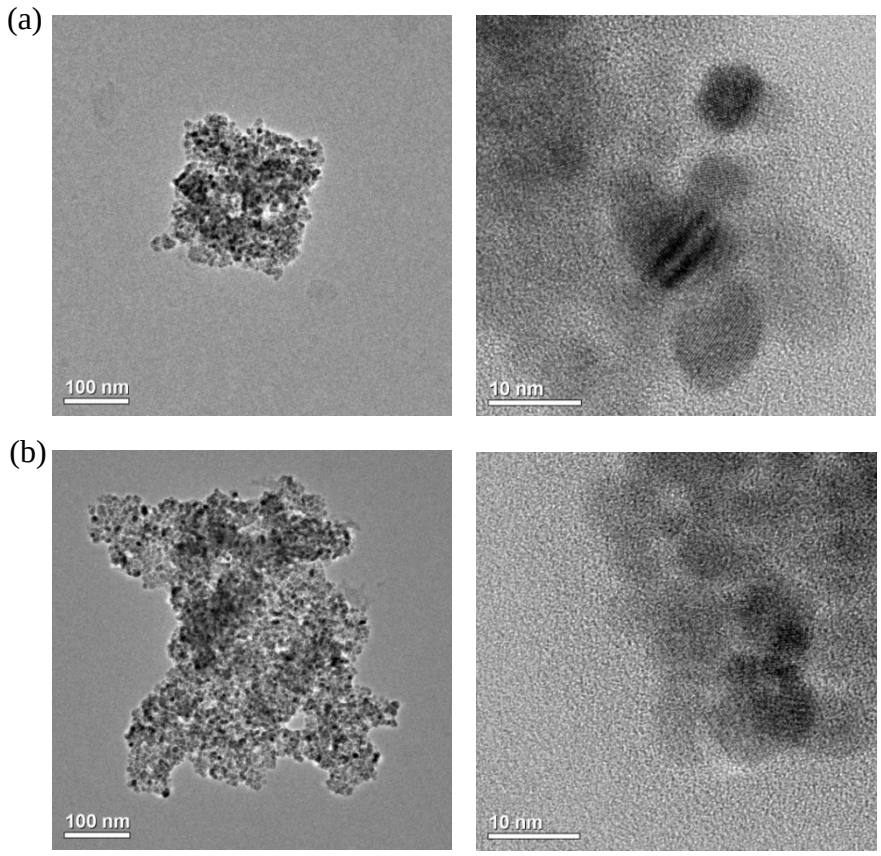

Figure 3.1. HR-TEM image of ferrofluids (a) EFH-1 (b) EFH-3

3.1.2. Thermogravimetric analysis

A thermogravimetric analysis of two types of ferrofluid shows weight losses with respect to temperature. For EFH-1, it was shown that there was an about 50% weight loss until 180°C and then the weight remained constant until 800°C, which indicates that the particles contained 50% magnetite.

For EFH-3, it was shown that there was smaller weight loss than EFH-1, indicating magnetic nanoparticles are contained up to 60 wt%. From the result, it appears that EFH-3 has much larger amount of magnetic nanoparticles than EFH-1, so it is found that saturation magnetization in EFH-3 is higher than that of EFH-1.

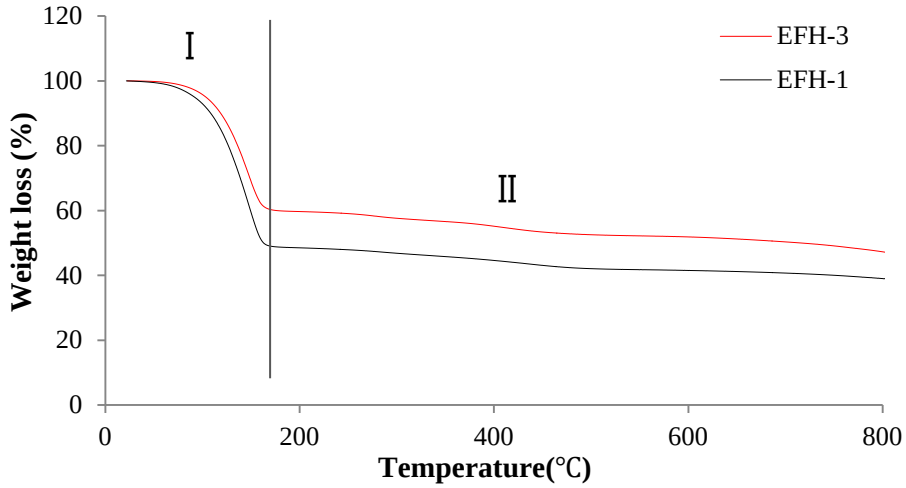

Figure 3.2. TGA curves of investigated ferrofluids

3.1.3. Magnetic field measurement

A pair of permanent magnets with a dimension of 400 mm × 250 mm × 100 mm was applied to produce static magnetic field. By using a gaussmeter, the magnetic flux densities were measured to be 200 mT, 300 mT, and 400 mT for one pair, two pairs and three pairs of the magnets, respectively. Depending on the location of the probe, the magnetic flux density was changed. Therefore, we measured the highest magnetic flux density under the external magnetic field. The measured values were used for simulating the ferrohydrodynamic energy harvesting system and setting an applied magnetic field on a rheometer.

3.2. Rheological properties of ferrofluid

3.2.1. Shear thinning behavior

Simple shear flow measurements were conducted at the shear rate from 0.01 s^{-1} to 500 s^{-1}. Fig.3.3 illustrates measured viscosity versus shear rate for EFH-1 at various magnetic fields. It was observed that the viscosity of EFH-1 decreased with increasing shear rate, showing the shear-thinning behavior. This shear thinning behavior was explained by the assumption that the nanoparticles in the ferrofluid cause formation and breakage of clustering chains [11].

At lower shear rate, random arrangement of particles caused an increase in the viscosity of the ferrofluid. However, at higher shear rate, magnetic particles begin to arrange their orientation along the direction of shear rate. Thus, the long chain-like structure leads to the decrease of the viscosity [12]. At above 100 s^{-1}, no change of the viscosity with the magnetic field appeared because most of the chain-like structures were broken and the particles were homogeneously distributed in the fluid.

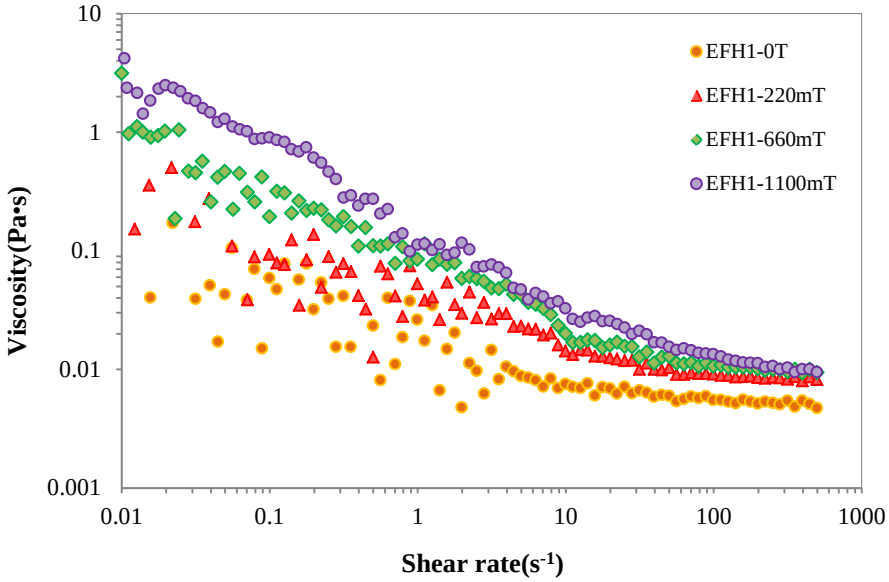

Figure 3.3. Variation in viscosity with shear rate at various magnetic fields for EFH-1

For EFH-3, the experiments were carried out using the rheometer adopting the same geometry and distance as used for EFH-1. The viscosity of EFH-3 was two times higher than that of EFH-1 because the concentration of the magnetic particles in EFH-3 was higher than that of EFH-1. In case of EFH-3, the shear thinning effect was also observed.

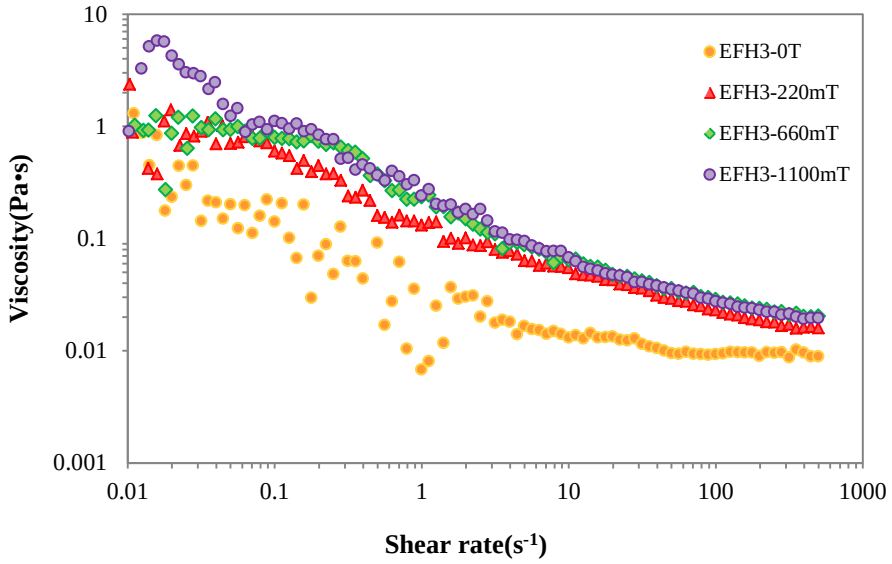

Figure 3.4. Variation in viscosity with shear rate at various magnetic fields for EFH-3

3.2.2. Magnetoviscous effect

From this result, it is shown that as magnetic field is increased, both EFH-1 and EFH-3 show the increase of the fluid's viscosity.

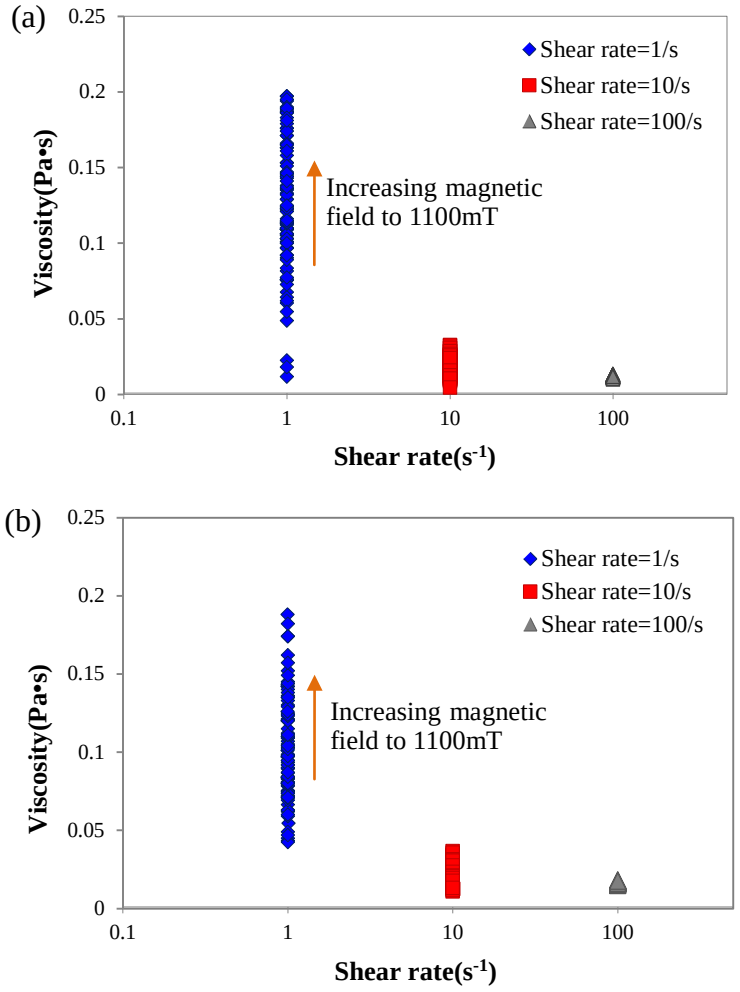

Figure 3.5. Shear rate VS viscosity for different magnetic field with increasing magnetic fields (a) EFH-1 (b) EFH-3

This phenomenon is called the “magnetoviscous effect”. The magnetoviscous effect was quantified by calculating the relative magnetic field-induced increase of the viscosity of the fluid (R) [13].

$$R = \frac{\eta(H) - \eta(H=0)}{\eta(H=0)}$$

The magnetoviscous effect for EFH-1 and EFH-3 is illustrated in Fig.3.7 and 3.8. A theoretical explanation of the effect given by Shliomis is based on the concept of the hindrance of rotation of the magnetic particles in a shear flow under an external magnetic field. In the presence of a magnetic field, the magnetic particles try to align along the magnetic field direction. However, under shear flow, the velocity gradient will induce a rotation of the magnetic particles, which causes a misalignment of the magnetic moments from the field direction. This leads to an increase in the viscosity of ferrofluid.

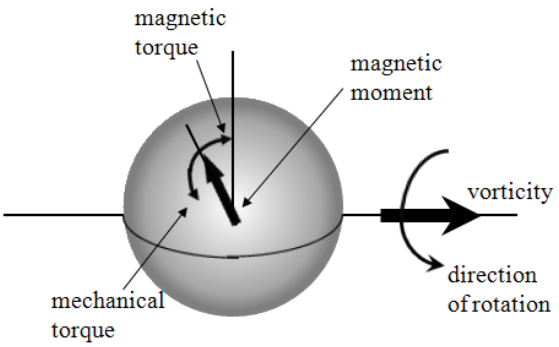

Figure 3.6. The origin of a field dependent increase of viscosity in a ferrofluid

In Fig.3.7, the magnetoviscous effect of EFH-1 represented 3000 % at lower shear rates and decreased with increasing shear rates, however, still remaining above 50 % for low magnetic fields.

For EFH-3, the magnetoviscous effect represented 3500 % at lower shear rates and still remained above 200 % for low magnetic fields at above 10 s^{-1}. The reason why the magnetoviscous effect of EFH-3 was higher than that of EFH-1 is that there were more magnetic particles in EFH-3 and the saturation magnetization of EFH-3 was higher than that of EFH-1.

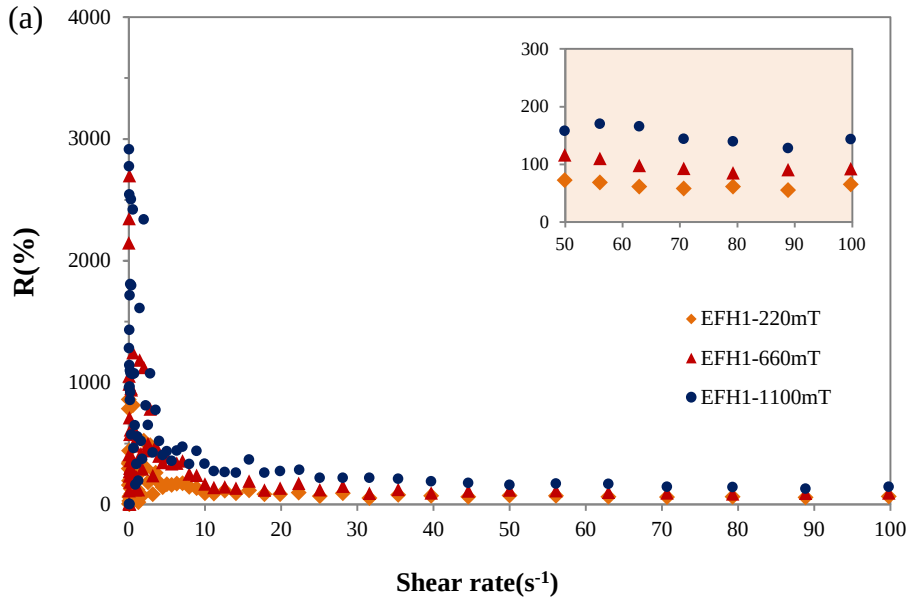

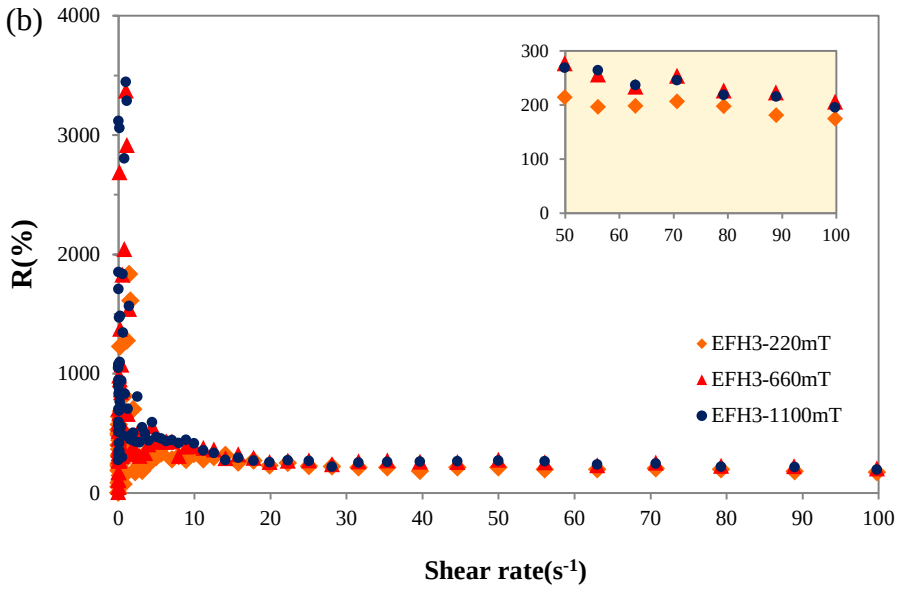

Figure 3.7. Magnetoviscous effect with various magnetic field (a) EFH-1 (b) EFH-3

3.2.3. Theoretical model of yield stress

In the absence of the external magnetic field, the EFH-1 and EFH-3 exhibited Newtonian fluid as shown in Fig.3.8. Dashed lines represent corresponding Newtonian fits.

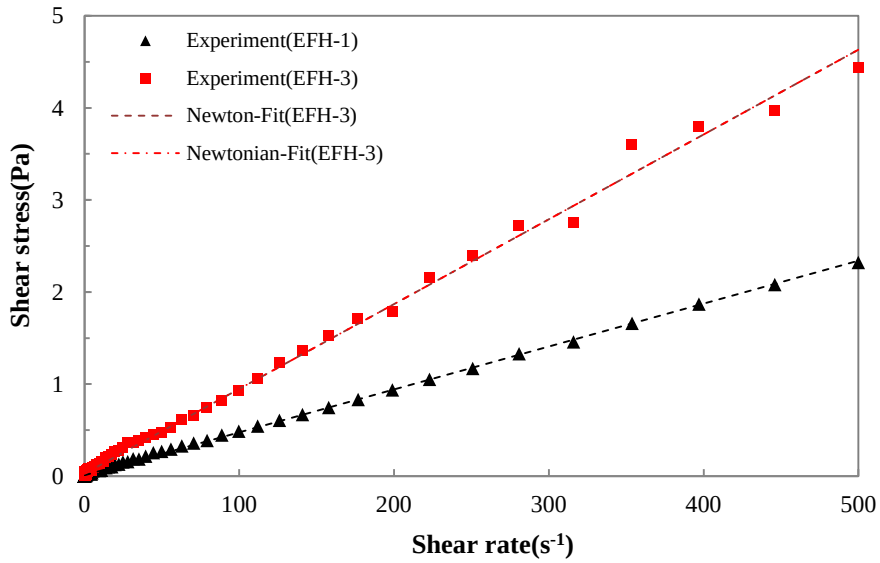

Figure 3.8. Shear stress versus shear rate in the absence of the magnetic field

Experiments with an external magnetic field led to a change in the ferrofluid's behavior. From Fig.3.9, we observed the rapid decrease of viscosity at low shear rates, which is related to the formation of new structures. According to this result, it is reasonable to suppose that EFH-1 and EFH-3 had yield stress.

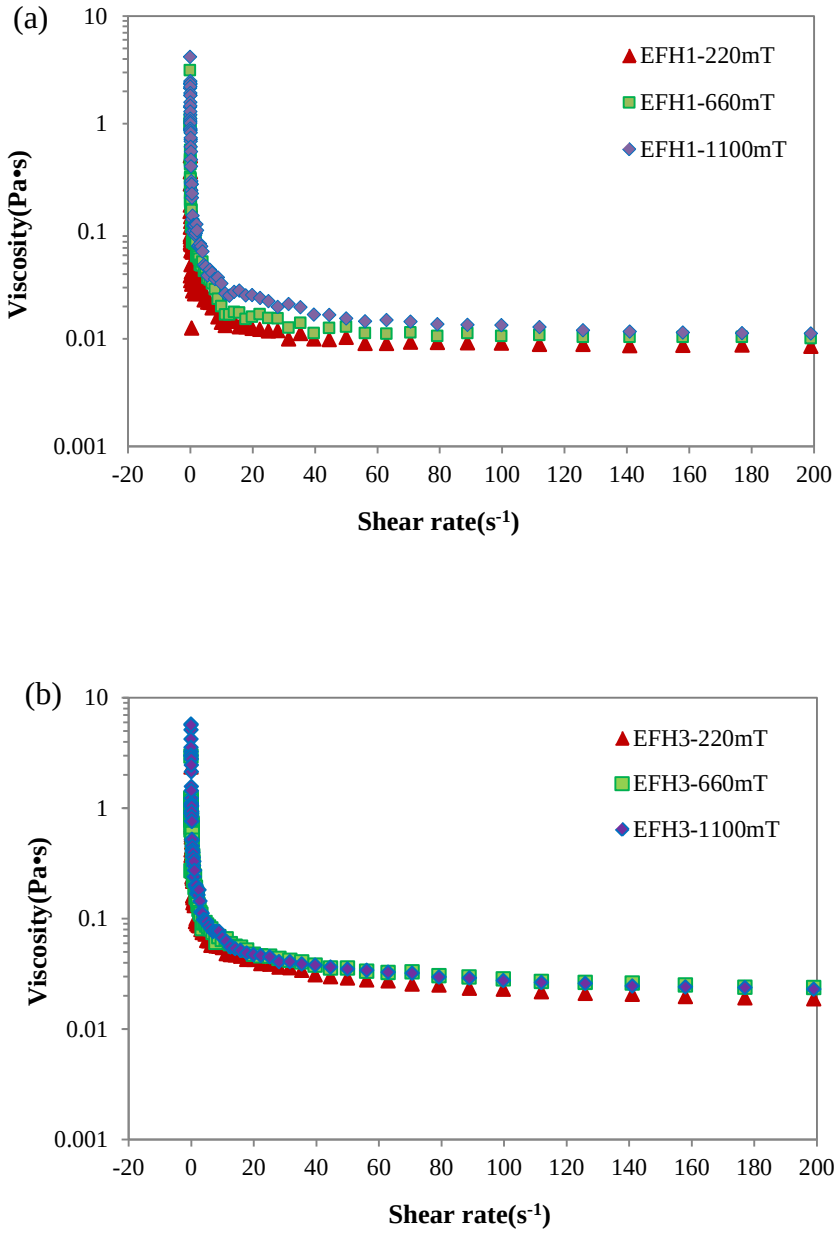

Figure 3.9. Viscosity versus shear rate under different magnetic fields

(a) EFH-1 (b) EFH-3

Yield stress is one of the most relevant rheological properties of magnetorheological fluid. Yield stress can be theoretically explained as an effect of the formation of structures in ferrofluid [14]. When a magnetic field is applied, the initial viscosity is increased in comparison to zero field state. This revealed that magnetic field causes the formation of the new structures [15].

Such behavior is usually well represented by a few theoretical models. One of the simplest theoretical models is the Bingham plastic model which takes account of the yield stress of fluids. The Bingham model is given by [16]:

$$\dot{\gamma} = 0 \qquad \text{if } \tau \leq \tau_{0,}$$
$$\tau = \tau_0 + \eta\dot{\gamma} \qquad \text{if } \tau > \tau_0$$

where τ_0 is the yield stress, η is the viscosity, and $\dot{\gamma}$ is the shear rate. This means when $\tau \leq \tau_0$, there is no fluid motion. Otherwise, the shear rate is directly proportional to the yield stress. The Bingham model was used to fit the measured data. The comparison of Bingham model with the experimental results is illustrated in Fig.3.10. Table 3.1. shows that as increasing magnetic field, the yield stress and viscosity of ferrofluid increased.

From Fig.3.10 and 3.11, the result of the experiment is that the yield stress of EFH-3 was always higher than EFH-1 at the same magnetic field regardless of suggested yield stress models. The reason is that EFH-3 contains more magnetic particles comparing with EFH-1.

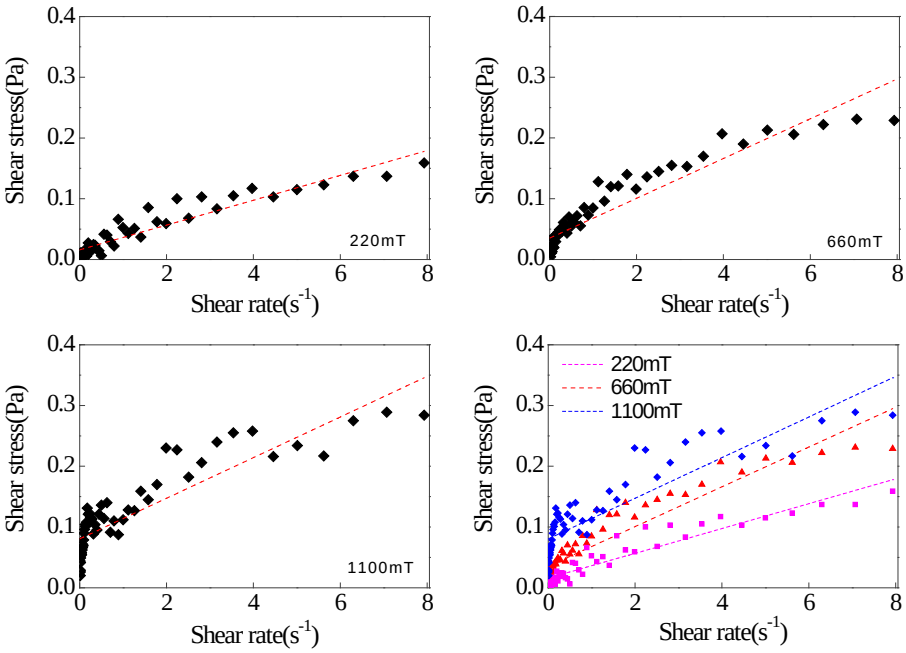

Figure 3.10. Shear stress of EFH-1 for different magnetic fields by using Bingham model

Table 3.1. Bingham fit parameters for EFH-1

Magnetic field	τ_0 (Pa)	η (Pa·s)
220mT	0.01571	0.02044
660mT	0.03506	0.03276
1100mT	0.08037	0.03346

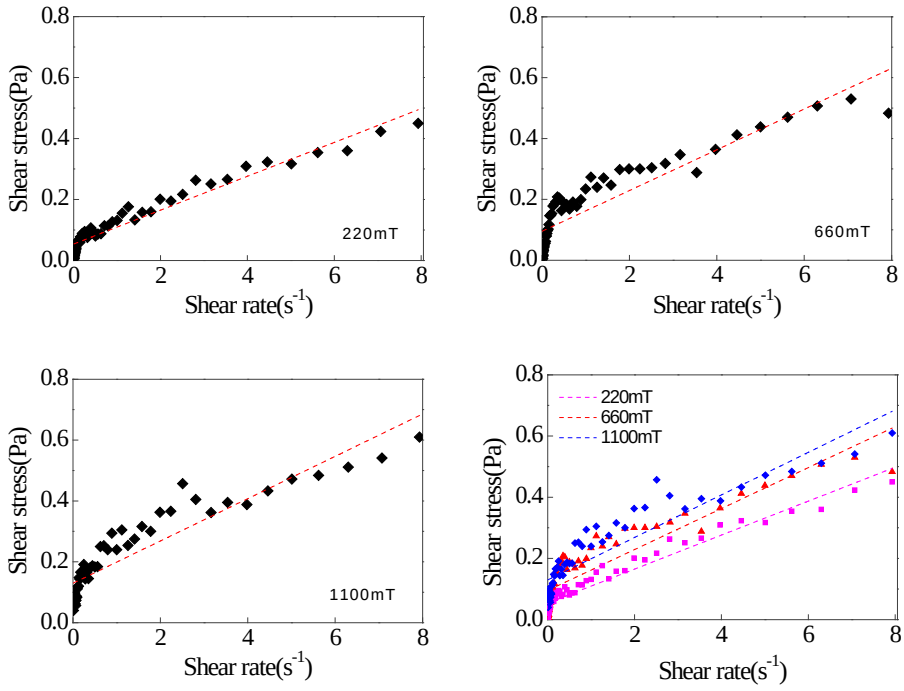

Figure 3.11. Shear stress of EFH-3 for different magnetic fields by using Bingham model

Table 3.2. Bingham fit parameters for EFH-3

Magnetic field	τ_0 (Pa)	η (Pa·s)
220mT	0.05386	0.05553
660mT	0.09489	0.06697
1100mT	0.1293	0.06955

The Casson model is based on the structure model of the interactive behavior of solid and liquid phases of a two-phase suspension. This model takes account of both yield stress and the shear-thinning behavior, adopting only two parameters.

$$\dot{\gamma} = 0, \qquad \text{if } \tau \le \tau_c,$$

$$\sqrt{\tau} = \sqrt{\tau_c} + \sqrt{\eta\dot{\gamma}}, \qquad \text{if } \tau > \tau_c$$

Here, τ_c is the Casson yield stress, and η is the constant viscosity as approaching to the infinite shear limit. For some viscous materials such as blood and food products, it provides better fit than the Bingham model.

A comparison of the Casson model with the experimental results for EFH-1 is illustrated in Fig.3.12. It seems that the Casson model is fitted better than the Bingham model. However, there was no tendency for yield stress and viscosity as the magnetic field was increased. The discrepancy can be explained by the low viscosity of ferrofluid which is unstable at lower shear rates.

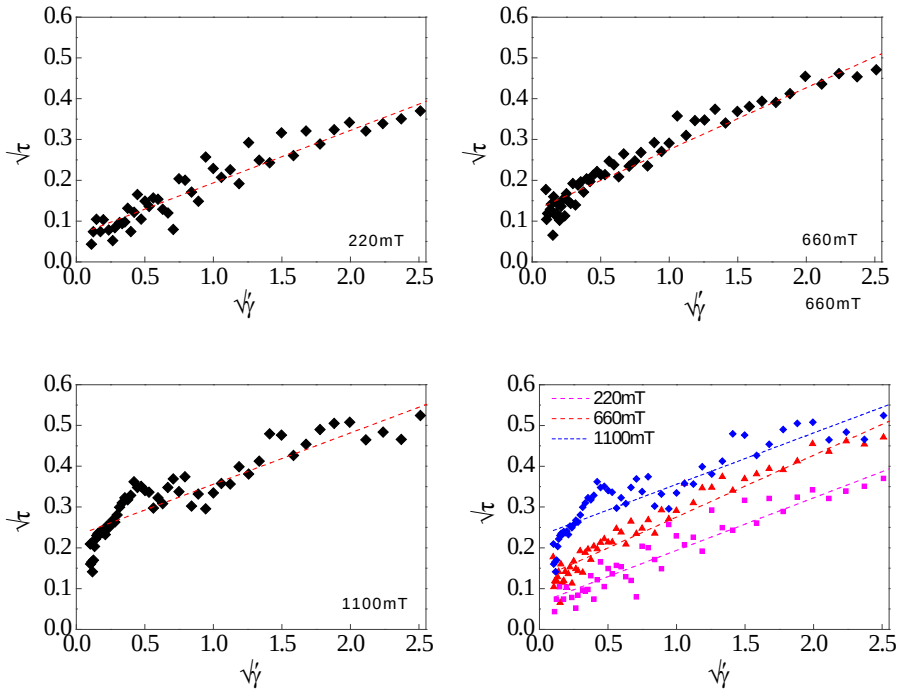

Figure 3.12. Shear stress of EFH-1 for different magnetic fields by using the Casson model

Table 3.3. Casson fit parameters for EFH-1

Magnetic field	$\sqrt{\tau}_c$	$\sqrt{\eta}$
220mT	0.06487	0.12877
660mT	0.012372	0.15161
1100mT	0.22957	0.12606

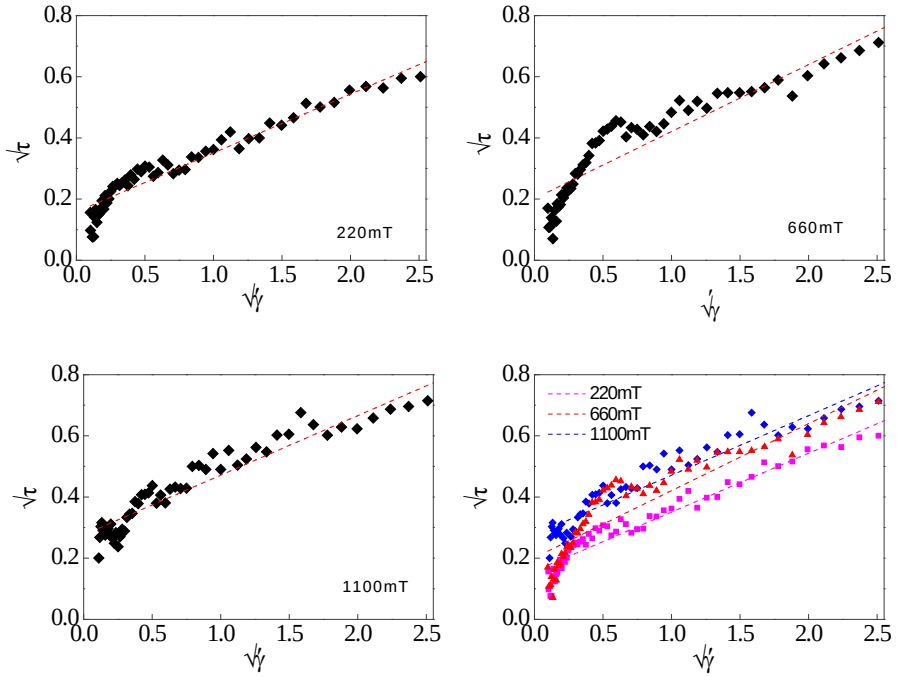

Figure 3.13. Shear stress of EFH-3 for different magnetic fields by using the Casson model

Table 3.4. Casson fit parameters for EFH-3

Magnetic field	$\sqrt{\tau}_c$	$\sqrt{\eta}$
220mT	0.15772	0.19265
660mT	0.20147	0.21919
1100mT	0.27629	0.19481

Another model for yield stress is the Herschel-Bulkley model which also takes account of both the yield stress and the shear-thinning effects, which is expressed as below [17]:

$$\tau = \tau_{HB} + k\dot{\gamma}^{n}$$

where τ_{HB} is the yield stress, k is the consistency parameter, and n is the power law index. When $\tau < \tau_{HB}$, the material behaves like a solid; otherwise, the material behaves as a power law fluid. The parameters n, τ_{HB}, and k for the Herschel-Bulkley model are listed in Table 3.5. The consistency parameter and yield stress increased with increasing magnetic field, while power law index decreased. The reason is that as the external magnetic field is increased, the particle begins to saturate. So, the yield stress is increased with the external magnetic field.

The best fit for the measured data was obtained by using the Herschel-Bulkley model in which correlation coefficient was the highest among these models. Therefore, the Herschel-Bulkley model is recommended as a suitable model for these magnetic nanofluids under external magnetic field.

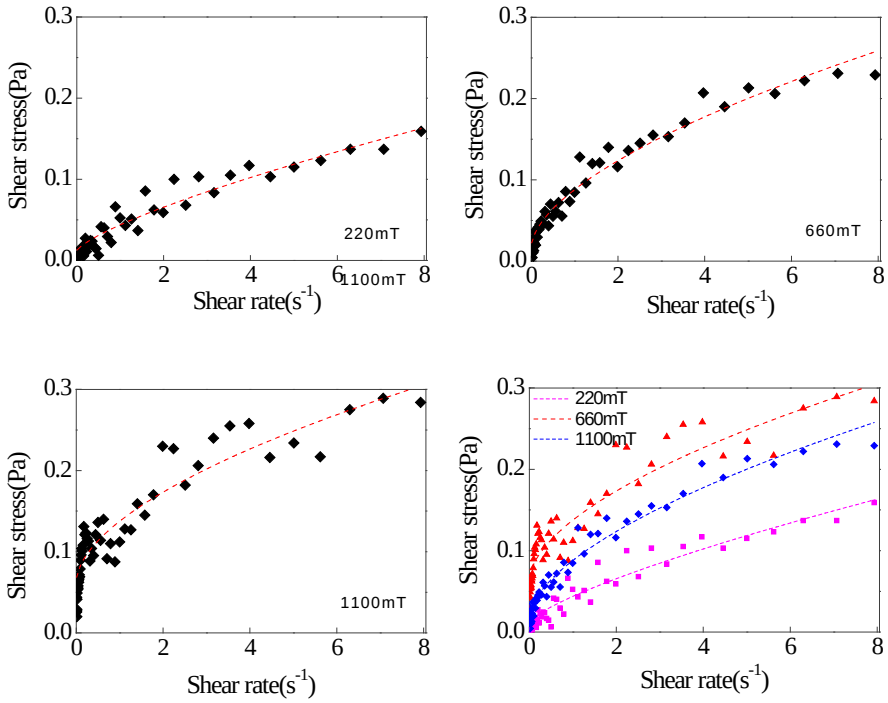

Figure 3.14. Shear stress of EFH-1 for different magnetic fields by using the Herschel–Bulkley model

Table 3.5. Herschel-Bulkley fit parameters for EFH-1

Magnetic field	τ_{HB} (Pa·s)	k	n
220mT	0.01168	0.03203	0.7479
660mT	0.01804	0.06985	0.05949
1100mT	0.06303	0.0744	0.56757

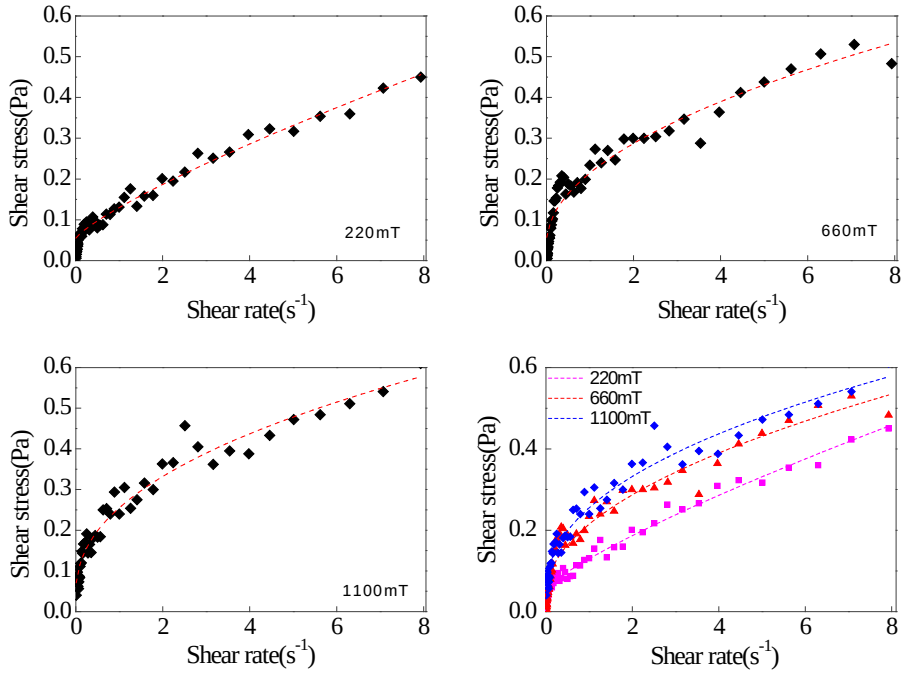

Figure 3.15. Shear stress of EFH-3 for different magnetic fields by using the Herschel–Bulkley model

Table 3.6. Herschel-Bulkley fit parameters for EFH-3

Magnetic field	τ_{HB} (Pa·s)	k	n
220mT	0.02066	0.11622	0.61379
660mT	0.04031	0.17447	0.50078
1100mT	0.0402	0.21491	0.44236

3.3. Output voltage and current

3.3.1. Effect of the flow rate of the air

When air-droplets were formed in ferrofluid, they caused the change of the magnetic flux through the coil. As a result, induced current and voltage were generated in the coil according to Faraday's law of induction. Fig.3.17 shows output current of the ferrohydrodynamic system for EFH-1.

This demonstrates the influence of the flow rate of air on the output current under the given magnetic field. It was observed that the output current was measured within the range from -0.01 mA to 0.01 mA regardless of the flow rate of air. However, the formation frequency of an air-droplet was changed with varying the flow rate of air. The average formation frequency of an air-droplet was 1 droplet per 22s, 7s, 3.5s, and 2s for 25 μl/min, 75 μl/min, 150 μl/min, and 250 μl/min, respectively.

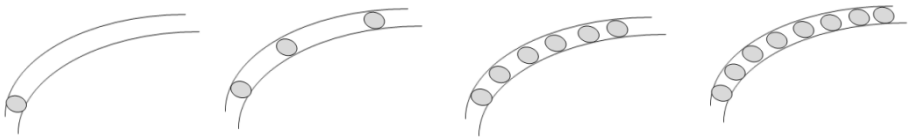

Figure 3.16. A schematic showing the distribution of the magnetic dipoles in the ferrofluid for different flow rate of air

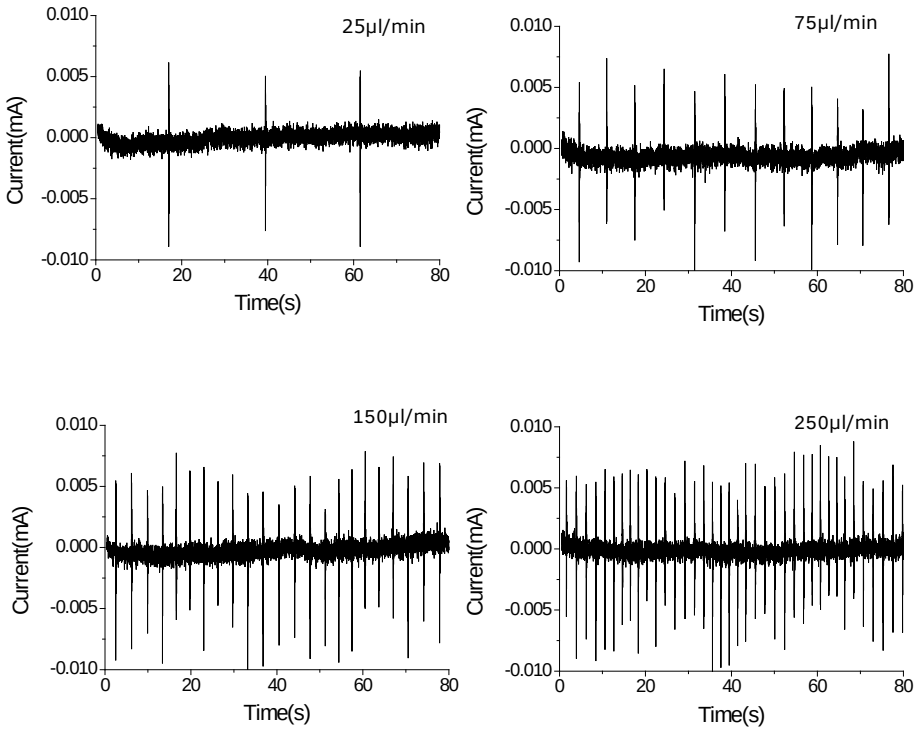

Figure 3.17. Effect of the flow rate of the air on output current

Fig.3.18 shows output voltage for EFH-1 ferrofluid. This result demonstrates the flow rate of air could not influence output voltage. It is suggested that the output voltage was constant regardless of increasing the flow rate of air because the flow rate of air changed only formation frequency of an air-droplet, not the time rate of change of the magnetic flux.

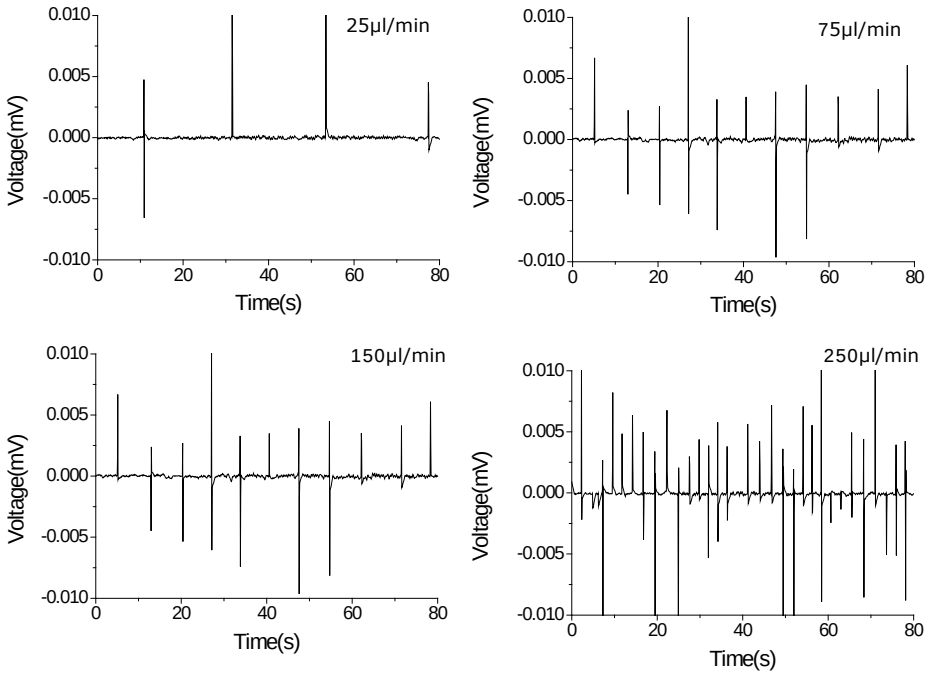

Figure 3.18. Effect of the flow rate of the air on output voltage

3.3.2. Effect of the magnetic field (H)

Fig.3.20 demonstrates an influence of the magnetic field on the output current for the given flow rate of air (75 μl/min). As mentioned above, both output current and voltage were not influenced by the flow rate of air. Therefore, it is valid to compare the magnetic field for given flow rate of air.

Fig.3.20-(a) shows the output current in the absence of the external magnetic field. It was observed that the output current showed noise signal only. This result was consistent with Faraday's law of induction which states the magnetic induction (B) is obtained by the relationship: $B=\mu_0(H+M)$. Since there was no applied magnetic field, both magnetic field (H) and magnetization (M) were zero despite movement of air-droplets in ferrofluid. As a result, no current was measured in the absence of the magnetic field.

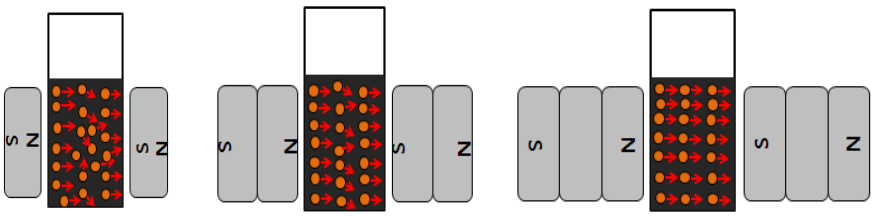

Figure 3.19. A schematic showing the distribution of the magnetic dipoles in a ferrofluid for different magnetic field

Fig. 3.20-(b~d) shows an output current with increasing magnetic field altered by changing the number of magnets. The output voltage

increased as increasing the number of magnets. This result demonstrates that increasing the magnetic field (H) influences magnetic flux (Φ_B) and finally increases induced current and voltage.

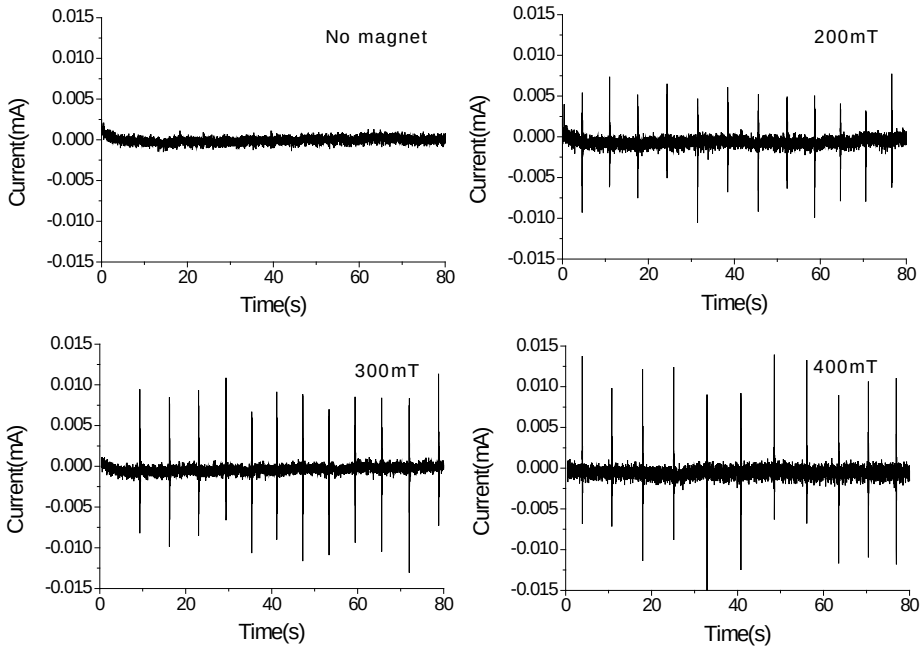

Figure 3.20. Effect of the magnetic field on output current

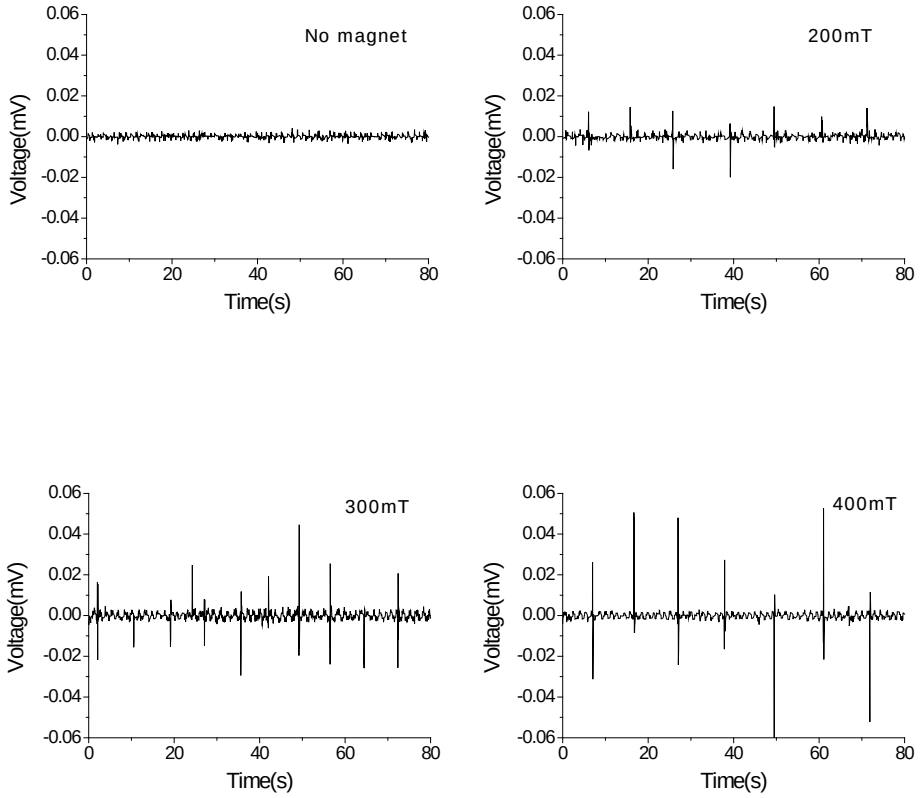

Figure 3.21. Effect of the magnetic field on output voltage

3.3.3. Effect of the magnetization (M)

To compare the effect of the magnetization, two different types of ferrofluid were used. The saturation magnetization of EFH-3 is higher than EFH-1. Typically, the saturation magnetization (M_s) was defined as the maximum of the magnetization value which is one of the most important and controversial properties of magnetic nanocrystals [18]. These ferrofluids have magnetic particles which are in the single-domain state, meaning that its internal magnetization is directed to the same direction. Therefore, it has the largest magnetic moment. As mentioned above, the size of magnetic particles for EFH-1 is similar to that of EFH-3. However, amount of magnetic particles for EFH-3 is more than that of EFH-1. It is that the reason why EFH-3 represented the higher saturation magnetization.

The comparison of output current between EFH-1 and EFH-3 is illustrated in Fig 3.22. The left side in Fig. 3.22 shows the output current for EFH-1 and the right side shows the output current for EFH-3. The results show that the output current for EFH-3 was always higher than that of EFH-1 no matter how much external magnetic field was applied in the coil. This result was consistent with Faraday's law of induction which states that the electromagnetic induction is influenced by not only the gradient of applied magnetic field but also magnetization.

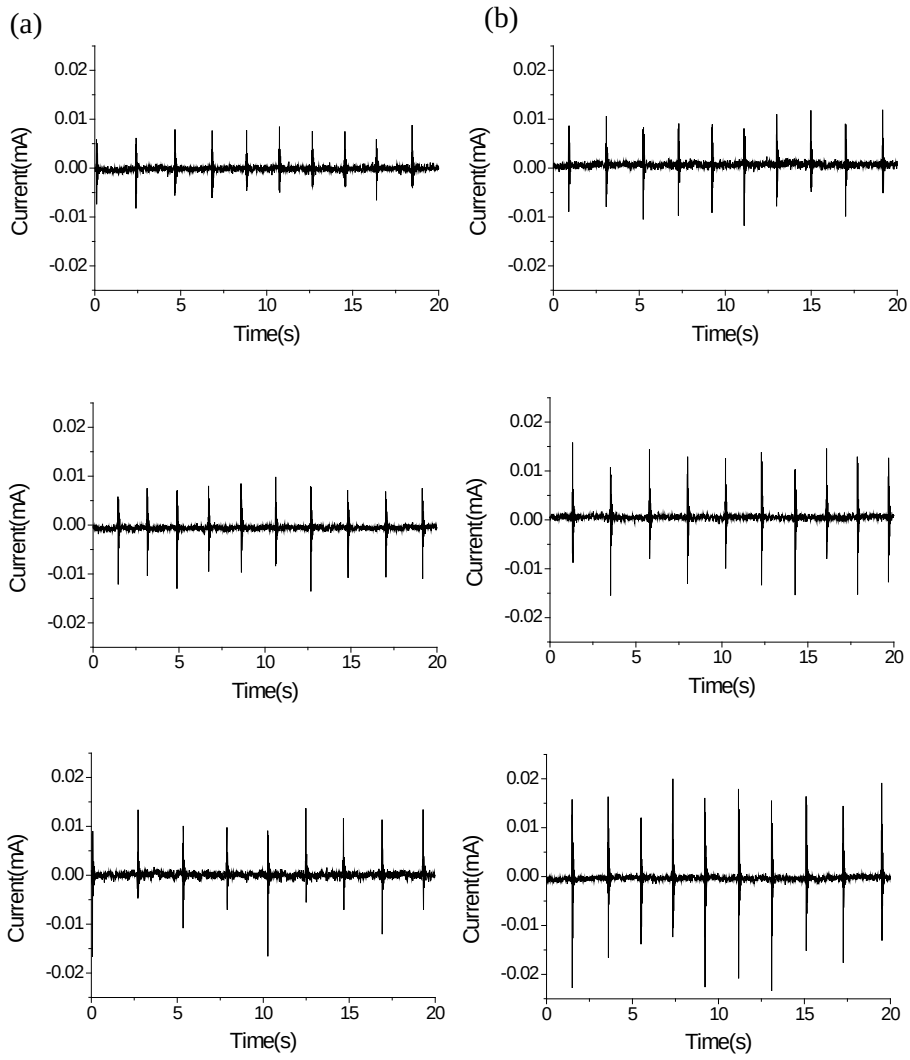

Figure 3.22. Effect of the magnetization on output current for (a) EFH-1 (b) EFH-3

3.4. Visualization of an air-droplet movement

Due to non-transparency of the ferrofluid, it could not be observed formation of air-droplets in the ferrofluid. To overcome this difficulty, transparent aqueous solution of PEO was used instead of the ferrofluid. Aqueous solution of PEO having the same viscosity of the ferrofluid was prepared in order to make the same condition for movement of air-droplets in the ferrofluid. Fig.3.23 shows that the viscosity of prepared aqueous solution of PEO was similar to that of ferrofluid.

The formation of an air-droplet was observed by a high speed camera as shown in Fig.3.24. It was observed that as time increased, an air-droplet was formed.

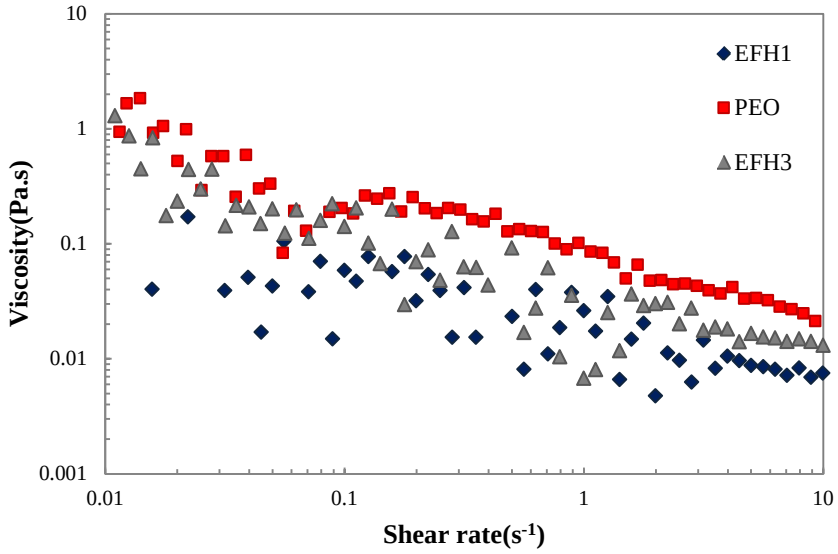

Figure 3.23. A comparison between viscosity of PEO and the ferrofluid

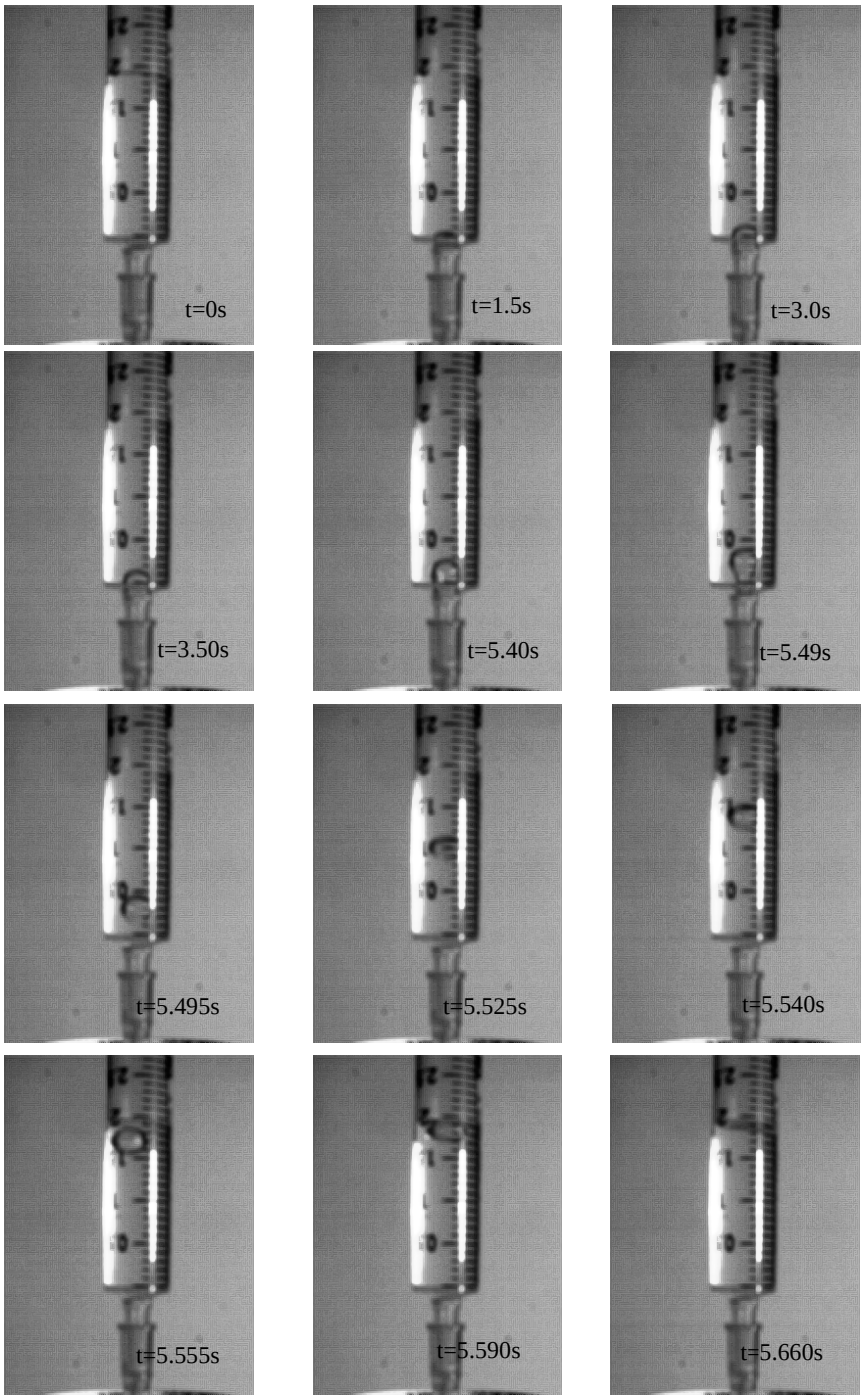

Figure 3.24. Illustration of formation of an air-droplet in aqueous solution of PEO

3.5. Numerical simulation

3.5.1. Governing equations

The governing equation of electrodynamics follows the Maxwell equation. Among the equation, Ampere's law was used and given by:

$$\nabla \times A = B$$

$$\sigma \frac{\partial A}{\partial t} + \nabla \times (\mu_0^{-1} \mu_r^{-1} B) - \sigma v \times B = J_e$$

$$\sigma \frac{\partial A}{\partial t} + \nabla \times (\mu_0^{-1} \mu_r^{-1} (B - B_{rem})) - \sigma v \times B = J_e$$

where the magnetic potential is A, the magnetic flux density is B, the externally generated current density is J_e, the electrical conductivity is σ, velocity is v, the magnetic permeability of air is μ_0, the relative permeability is μ_r, and the remnant magnetic flux density is B_{rem}.

Among constitutive relations, Remnant constitutive equation was used for the simulation because the differences in geometry between cylindrical multi-coil and rectangular magnet make the numerical simulation complicated. Remnant constitutive law the magnet is given by:

$$B = \mu_0 \mu_r H + B_{rem}$$

where μ_0 is the magnetic permeability of air, μ_r is the relative magnetic permeability of the permanent magnet, H is the magnetic field, B is the magnetic flux density, and B_{rem} is the remnant magnetic flux density[19].

For numerical simulation, we alternatively considered movement of an air-droplet by remeshing the air-droplet domain followed by the droplet movement in a height direction. The remnant magnetic flux was set as follows. Remnant flux density for r-directions was used by following the measured value in the system with one pair of magnets.

Remnant flux density (B_{rem}): r-direction: 0.2 [T]

φ-direction: 0 [T]

z-direction: 0 [T]

The boundary conditions were applied as symmetry plane at z = 0. Magnetic insulation boundary conditions are set as follows [20]; $n \times A = 0$

3.5.2. Homogenization of the calculation domain

To solve the problem, we assumed a 2D axisymmetric model where the modeling domain is a rectangular region in the rz-plane bounded by the magnetic insulation boundary conditions. We assumed a simple geometry because the differences in geometry of a cylindrical multi-coil and a rectangular magnet make numerical simulation complicated. The geometry is shown in Fig.3.25.

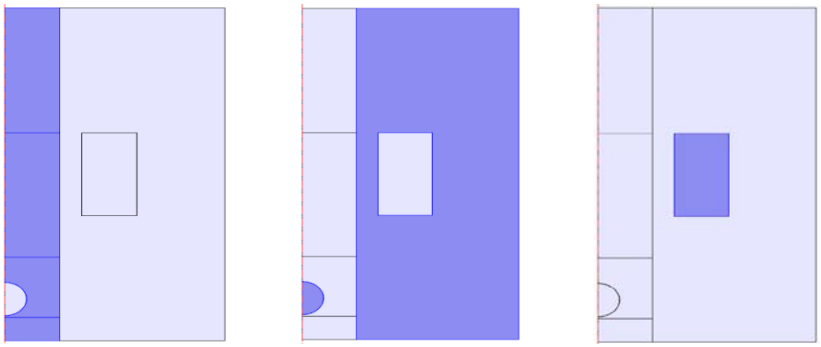

Figure 3.25. Illustration of simulation domain: The colored region represented (a) Magnetized region (b) air (c) Multi-turn coil

Due to complex coil structure wound with several turns, the coil cross section needs homogenization.

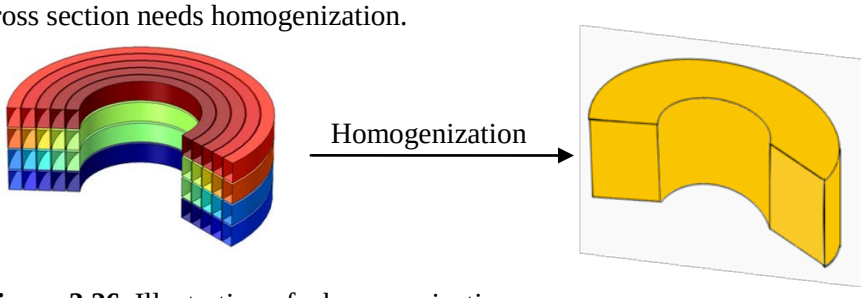

Figure 3.26. Illustration of a homogenization process

3.5.3. Numerical solutions

Axial movement of air-droplets through the center of the coil induced an output voltage across the coil. Fig.3.27 shows the magnetic flux density and the magnetic flux field over time. According to the Maxwell equation, it was observed the magnetic flux was changed with time. Fig.3.28-(b) shows the induced voltage in the multi-turn coil estimated by simulation. The output voltage estimated by the simulation was in the range from -2×10^{-5} V to 8×10^{-5} V. Although there is the discrepancy of the magnitude of the induced voltage between experiment and simulation, it can be explained assumptions about geometry and remnant constitutive equation.

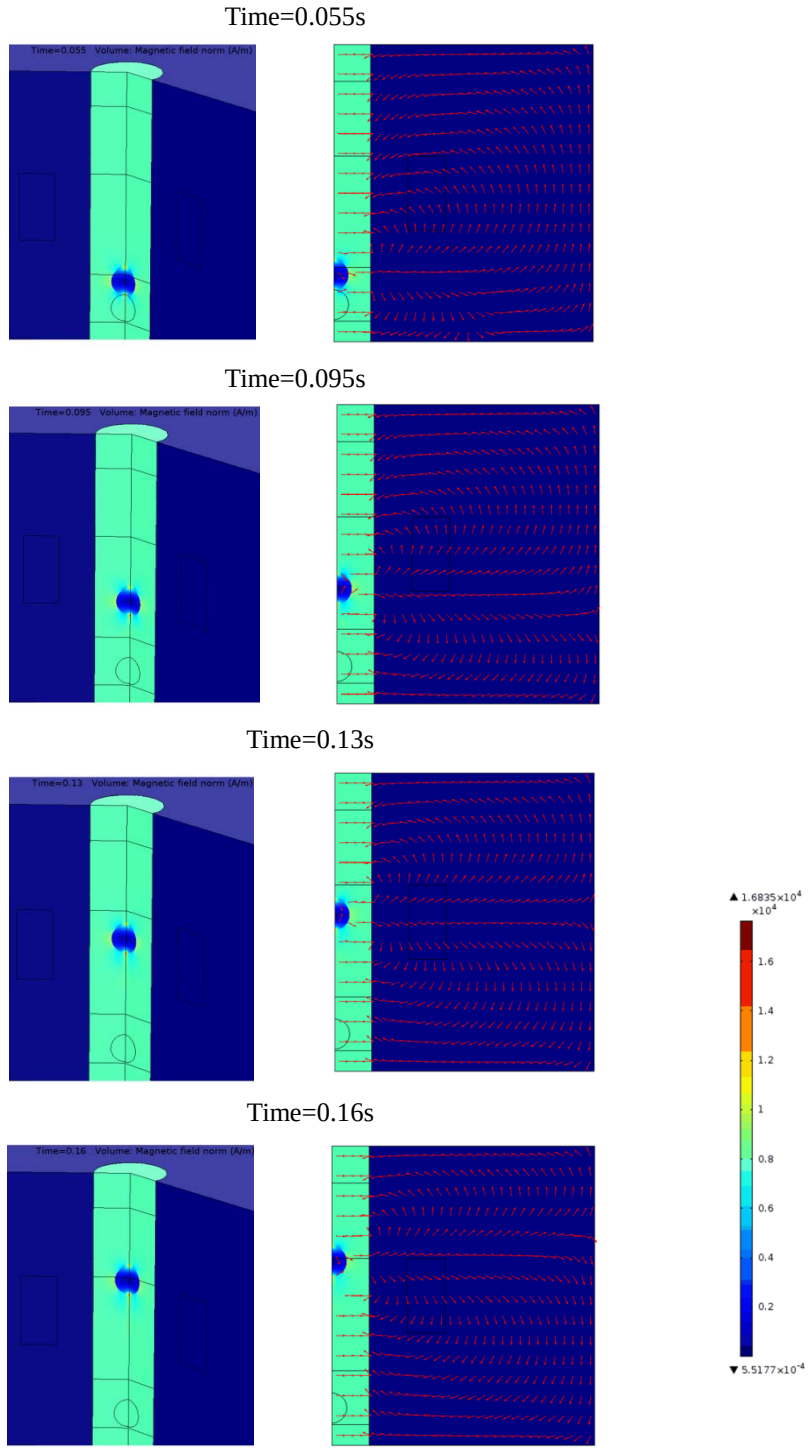

Figure 3.27. Magnetic flux density and magnetic flux field over time

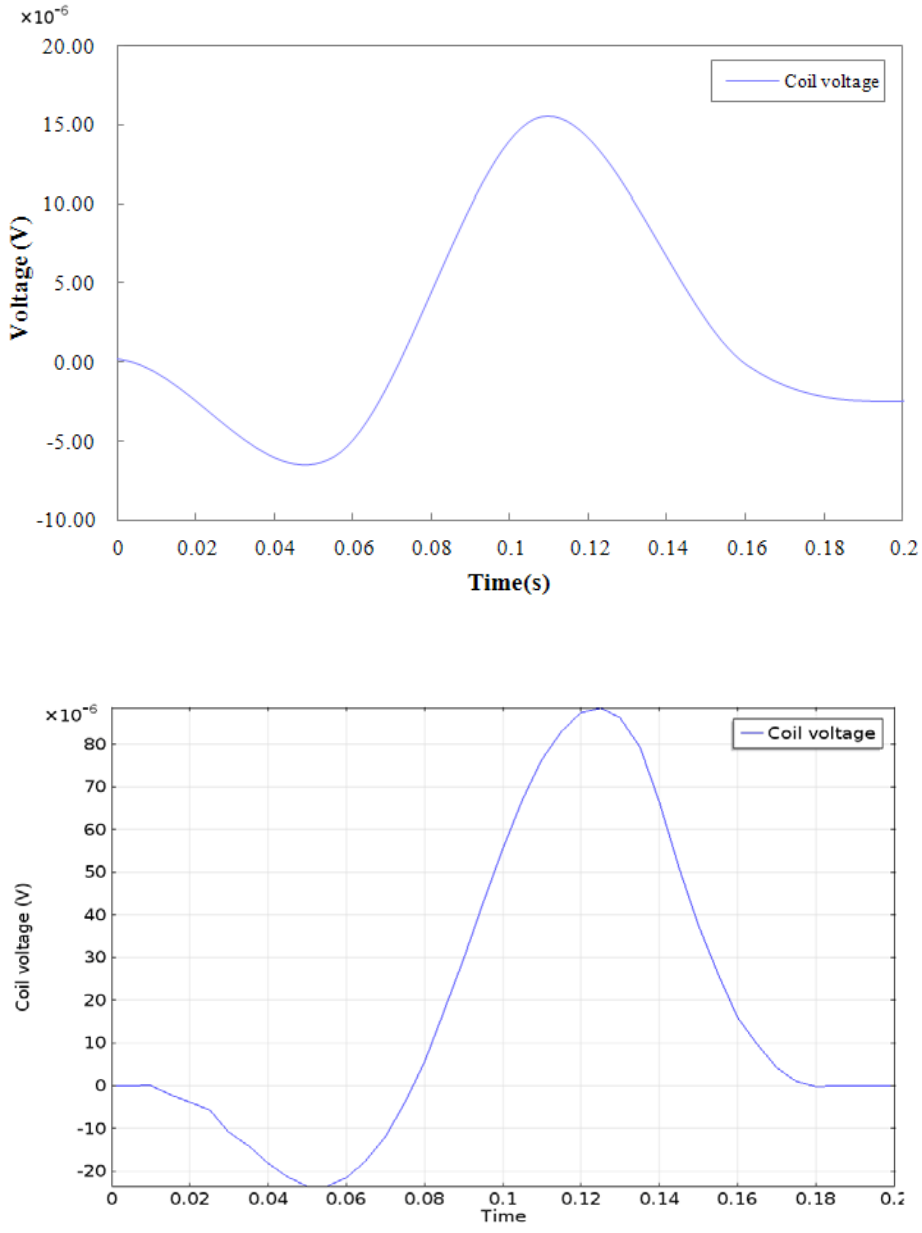

Figure 3.28. (a) Experimental and (b) simulation results of induced voltage over time.

Ⅴ. CONCLUSION

In this study, we characterized the magnetorheological and magnetodynamic effects on both of EFH-1 and EFH-3 ferrofluid. It was found that ferrofluids showed remarkable shear thinning and magnetoviscous effect under magnetic field. It becomes obvious that magnetic nanoparticles inside the ferrofluids form nanoclustering and chain-like structure under the magnetic field since they uniquely represents superparamagnetic characteristics due to their nano-scale morphology.

The ferrofluids also showed yield stress behavior under the magnetic field. However, the saturation magnetization of ferrofluids limited to reach the expected theoretical values.

Owing to the magnetorheological and magnetodynamic effects, our ferrohydrodynamic system was proposed for an energy harvesting platform. The output voltage and current were measured depending on the flow rate of air, the magnetic field (H), and the magnetization (M). It was observed that the output voltage and current were increased with increasing the magnetic field (H) and magnetization (M) for the ferrohydrodynamic system.

The ferrohydrodynamic system has a lot of advantages comparing with the conventional electromagnetic energy harvesting systems. First, unlike conventional electromagnetic generators that use a permanent solid magnet, a ferrofluid can be used where the solid magnet cannot be utilized in

complex shapes and geometries. In addition, the novel ferrohydrodynamic system utilizes movement of air-droplets in a ferrofluid so that only a small amount of input energy source is needed unlike the conventional energy harvesting systems based on vibrating or oscillating motions. We believe a newly proposed energy harvesting concept is very promising for developing an electromagnetic energy harvesting platform and understanding physical insight based on magnetorheology and magnetodynamics.

REFERENCES

[1] T.A. Franklin, *Ferrofluid Flow Phenomina*, Massachusetts Institute of Technology, Department of Electrical Engineering and Computer Science (2003)

[2] A.R. Muxworthy, and W. Williams, *Journal of the Royal Society Interface*, **6**, 1207 (2009)

[3] M. Osaci, *Journal of Magnetism and Magnetic Materials* (2013)

[4] C. Scherer, and A.M. Figueiredo Neto, *Brazilian Journal of Physics*, **35**, 718 (2005)

[5] C. Rinaldi, A. Chaves, S. Elborai, X. He, and M. Jahn, *Current Opinion in Colloid & Interface Science*, **10**, 141 (2005)

[6] M.M. Abid, Spacecraft Sensors, John wiley & Son,Ltd (2005)

[7] W. Greiner, *Classical electrodynamics*, Springer-Verlg (1998)

[8] R.J.M. Vullers, R. van Schaijk, I. Doms, C. Van Hoof, and R. Mertens, *Solid-State Electronics*, **53**, 684 (2009)

[9] M. Mizuno, and D.G. Chetwynd, *J. Micromech. Microeng.*, **13**, 209 (2003)

[10] P. D. Mitcheson, E. M. Yeatman, G.K. Rao, A.S. Holmes, and T.C. Green, Proceedings of the IEEE, **96**, 1457 (2008)

[11] S. Odenbach, *Colloids and Surfaces A*, **217**, 171 (2003)

[12] R.Y. Hong, Z.Q. Ren, Y.P. Han, H.Z, Li, Y. Zheng, and J. Ding, *Chemical Engineering Science*, **62**, 5912 (2007)

[13] J. Nowak, and S. Odenbach, *IEEE TRANSACTIONS ON MAGNETICS*, **49**, 208 (2013)

[14] H. Shahnazian, and S. Odenbach, *International Journal of Modern Physics B*, **21**, 4806 (2007)

[15] E. Ghasemi, A. Mirhabibi, and M. Edrissi, *Journal of Magnetism and Magnetic Materials*, **320**, 2635 (2008)

[16] H. Zhu, Y.D. Kim, and D. De Kee, *J. Non-Newtonian Fluid Mech.* **129**,177 (2005)

[17] Q. D. Nguyen, and D. V. Boger, *Annual Review of Fluid Mechanics*, **24**, 47 (1992)

[18] H. M. Lu, W. T. Zheng, and Q. Jiang, *Journal of Physics D,* **40**, 320 (2007)

[19] A. M. Morega, A. A. Dobre, and M. Morega, *Numerical Simulation of Magnetic Drug Targeting with Flow- Structural Interaction in an Arterial Branching Region of Interest*, the Proceedings of the COMSOL Conference (2010)

[20] A. Alferenok, A. Poth´erat and U. Luedtke1, M*easurement science and technology,* **24,** 13 (2013)

국문 요약

최근 에너지 하베스팅에 대한 관심이 집중되고 있다. 특히 전자기에너지를 이용하는 에너지 하베스팅 연구에 관한 관심은 더욱더 높아지고 있으며 실제응용분야를 고려하지 않더라도 실험실을 기반으로 한 많은 연구들이 개발되고 있다. 본 연구에서는 액체자석 내에서 움직이는 기포를 이용하여 에너지 하베스팅 플랫폼을 제안하였다. 패러데이 법칙은 외부 자기장 하에서 자기선속의 변화로 인하여 코일 내에 유도기 전압을 발생시킨다는 법칙이다. 이 법칙을 기반으로 페로하이드로다이나믹 시스템이 만들어졌다.

유도전압과 전류는 공기의 유속, 자기장의 세기, 자기화를 변화시켜가며 측정하였다. 첫 번째 실험을 통해 공기의 유속과는 상관없이 출력전류와 전압이 일정한 범위에서 나오는 결과를 확인하였다. 두 번째 실험으로는 자석의 개수를 늘려가며 외부 자기장의 세기를 증가시켰으며, 이에 따라 출력 전압과 전류가 증가하는 것을 확인하였다. 마지막으로는 서로 다른 자화도를 가진 물질을 사용하여 출력전압과 전류를 측정하였으며, 높은 자화도를 가진 물질로부터 더 높은 출력전압과 전류 값이 얻어진다는 결과를 확인하였다. 또한 COMSOL 을 이용한 수치해석을 통해 에너지 하베스팅을 위한 페로하이드로다이나믹 시스템 내에서 유도전압과 전류를 발생한다는 것을 증명하였다.

이번 연구에서는 두 가지 종류의 액체자석의 자기유변학적과 자기다이나믹 효과를 분석하였다. 외부 자기장 하에서 액체자석이 shear thinning effect, magnetoviscous effect 을 나타낸다는 것을 확인하였다.

주요어 : 페로하이드로다이나믹, 자성유체, 액체자석, 에너지 하비스팅, 전자기학

학번 : 2011-23319